

Influence of Ocean Alkalinity Enhancement with Olivine or Steel Slag on a Coastal Plankton Community in Tasmania

Jiaying A. Guo^{1,2}, Robert F. Strzepek², Kerrie M. Swadling^{1,2}, Ashley T. Townsend³, Lennart T. Bach¹

¹Institute for Marine and Antarctic Studies, University of Tasmania, Hobart, Tasmania, 7000 Australia

²Australian Antarctic Program Partnership (AAPP), Institute for Marine and Antarctic Studies, University of Tasmania, Hobart, Tasmania, 7000 Australia

³Central Science Laboratory, University of Tasmania, Sandy Bay, Tasmania, 7005 Australia

Correspondence to: Jiaying A. Guo (Jiaying.guo@utas.edu.au)

Abstract. Ocean alkalinity enhancement (OAE) aims to increase atmospheric CO₂ sequestration in the oceans through the acceleration of chemical rock weathering. This could be achieved by grinding rocks containing alkaline minerals and adding the rock powder to the surface ocean where it dissolves and chemically locks CO₂ in seawater as bicarbonate. However, CO₂ sequestration during dissolution coincides with the release of potentially bio-active chemicals and may induce side effects. Here, we used 53 L microcosms to test how coastal plankton communities from Tasmania respond to OAE with olivine (mainly Mg₂SiO₄) or steel slag (mainly CaO and Ca(OH)₂) as alkalinity sources. Three microcosms were left unperturbed and served as a control, three were enriched with olivine powder (1.9 g L⁻¹), and three with steel slag powder (0.038 g L⁻¹). Olivine and steel slag powders were of similar grain size, but the amount of added olivine needed to be much higher than the steel slag because less alkalinity is released by the olivine than the steel slag over the 3-week experiment. Phytoplankton and zooplankton community responses as well as some biogeochemical parameters were monitored for 21 days. Olivine and steel slag additions increased total alkalinity by 29 μmol kg⁻¹ and 361 μmol kg⁻¹ respectively, which corresponds to a theoretical increase of 0.9 % and 14.8 % of the seawater storage capacity for atmospheric CO₂. Olivine and steel slag released silicate nutrients into the water column, but steel slag released considerably more and also significant amounts of phosphate. After 21 days, no significant difference was found in dissolved iron concentrations (>100 nmol L⁻¹) in the treatments and the control. Both minerals released dissolved aluminium (>50400 nmol L⁻¹). The slag addition increased dissolved manganese concentrations (771784 nmol L⁻¹), while olivine increased dissolved nickel concentrations (378 nmol L⁻¹). The slag treatment increased the total particulate manganese concentrations (22.2 nmol L⁻¹), while olivine increased the total particulate nickel (5.29 nmol L⁻¹), which was consistent with the increase in the dissolved concentrations of these trace metals in seawater. There was no significant difference in total chlorophyll *a* concentrations between the treatments and the control, likely due to nitrogen limitation of the phytoplankton community. However, flow cytometry results indicated an increase in the cellular abundance of several smaller (~<20 μm) phytoplankton groups in the olivine treatment compared to the slag treatment and the control. The abundance of larger phytoplankton (~>20 μm) decreased much more in the control than in the mineral addition treatments after day 10. Furthermore, the maximum quantum yields of photosystem II (F_v/F_m) were higher in slag and olivine treatments, suggesting that mineral additions increased photosynthetic performance. The zooplankton community composition was also affected with the most notable changes being observed in the dinoflagellate *Noctiluca scintillans* and

37 the appendicularian *Oikopleura* sp. Overall, steel slag is much more efficient for CO₂ removal with OAE than olivine and
38 appears to induce less change in the plankton community when relating the CO₂ removal potential to the level of
39 environmental impact that was observed here.

40

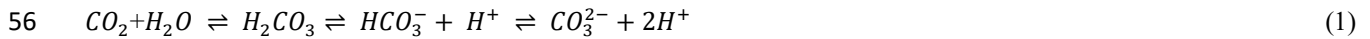
41 **1 Introduction**

42 Keeping global warming below 2 °C requires immediate emissions reduction. Additionally, between 450-1100 Gigatonnes
43 of carbon dioxide (CO₂) need to be removed from the atmosphere by 2100 (Smith et al., 2023). This could be achieved
44 with a portfolio of terrestrial and marine Carbon Dioxide Removal (CDR) methods. Ocean alkalinity enhancement (OAE)
45 is a marine CDR method that could theoretically contribute significantly to the global CDR portfolio (Ilyina et al., 2013;
46 Feng et al., 2017; Lenton et al., 2018).

47

48 Alkalinity is generated naturally when rock weathers and it has control on the ocean's chemical capacity to store CO₂
49 (Schuiling and Krijgsman, 2006). Natural rock weathering is currently responsible for about 0.5 Gt of atmospheric CO₂
50 sequestration every year (Renforth and Henderson, 2017). The idea behind OAE is to accelerate natural rock weathering
51 by extracting calcium- or magnesium-rich rocks, such as olivine, pulverizing them, and spreading them onto the sea surface
52 to increase chemical weathering rates (Hartmann et al., 2013). The weathering (i.e., dissolution) of these alkaline minerals
53 will consume protons (H⁺), which shifts the carbonate chemistry equilibrium in seawater from CO₂ towards increasing
54 bicarbonate (HCO₃⁻) and carbonate ion (CO₃²⁻) concentrations:

55



57

58 thereby making new space for atmospheric CO₂ to be dissolved in seawater and permanently stored. Previous model studies
59 have shown that OAE can mitigate climate change significantly by increasing the oceanic uptake of CO₂ from the
60 atmosphere (Kohler et al., 2010; Paquay and Zeebe, 2013; Keller et al., 2014; Lenton et al., 2018). For example, the study
61 by Burt et al. (2021) suggested that the total global mean dissolved inorganic carbon (DIC) inventories would increase by
62 156 GtC after total alkalinity is enhanced at a rate of 0.25 Pmol year⁻¹ in 75-year simulations.

63

64 There are a variety of alkaline minerals that could be used for OAE. A widely considered naturally occurring mineral is
65 forsterite, a (Mg₂SiO₄)-rich olivine. This type of olivine is abundant in ultramafic rock such as dunite, constituting at least
66 88 % of the rock composition (Ackerman et al., 2009; Su et al., 2016). Olivine occurs in the Earth's crust but is more
67 abundant in the upper mantle. There are at least several billion tons of olivine resources on Earth (Caserini et al., 2022).
68 However, the extraction of olivine in 2017 was only around 8.4 Mt year⁻¹ (Reichl et al., 2018), which is about two orders
69 of magnitude below the mass needed for climate-relevant OAE with olivine (Caserini et al., 2022). The net reaction for
70 CO₂ sequestration with Mg₂SiO₄ is:

71

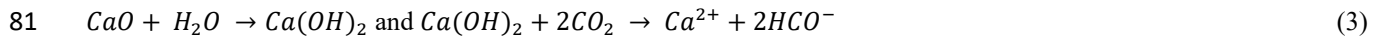


73

74 Another potential OAE source material is steel slag (Renforth, 2019), a by-product of steel manufacturing. During steel

75 manufacturing, high-purity calcium oxide (CaO) is used to improve the quality of the steel through accumulation of
76 unwanted materials such as sulphur and phosphorus. Steel slag mainly contains CaO, SiO₂, Al₂O₃, Fe₂O₃, MgO, and MnO
77 (Kourounis et al., 2007), and the chemical composition can vary depending on the manufacturing process (Wang et al.,
78 2011). Due to the presence of CaO and potentially other alkaline components, steel slag can increase alkalinity when
79 dissolved in seawater. The chemical reaction for CO₂ sequestration with CaO is:

80



82

83 Some of the steel slag that is produced during steel manufacturing is further used (e.g., for road construction and civil
84 engineering) but in some countries like China, 70.5 % of steel slag is left unused and stored in dumps (Guo et al., 2018).
85 In 2016, more than 300 million tons of steel slag was not used effectively, thereby occupying the land and raising
86 environmental concerns (Guo et al., 2018). The effective alkaline composition, availability, and relatively low cost of the
87 raw materials make olivine and steel slag potential source materials for OAE.

88

89 To assess whether OAE is viable, it needs to be understood how its application may affect marine biota such as plankton
90 and the biogeochemical fluxes they drive. Some data on the effects of OAE with sodium hydroxide (NaOH) on plankton
91 communities have recently been published (Ferderer et al., 2022; Subhas et al., 2022), but to the best of our knowledge, no
92 such data ~~is~~ are available for olivine- and/or slag-based OAE. Chemical perturbations via olivine and slag should be like
93 those by NaOH in that they increase seawater pH and shift the carbonate chemistry equilibrium (see Eq. 1). However, there
94 would be additional chemical perturbations because minerals contain a variety of potentially bioactive elements that are
95 released into the environment when they dissolve in seawater (Bach et al., 2019). One particular concern is that natural and
96 anthropogenic minerals such as olivine and steel slag are rich in bioactive metals that are usually scarce in the ocean, such
97 as iron (Fe), copper (Cu), nickel (Ni), manganese (Mn), zinc (Zn), cadmium (Cd), and chromium (Cr). Many of these trace
98 metals are essential micronutrients for phytoplankton growth (Sunda, 2000; Sunda, 2012), such as being co-factors for
99 various metalloenzymes (summarized by Twining and Baines, 2013). It is possible that the addition of alkaline minerals
100 may benefit phytoplankton by providing trace metals currently limiting phytoplankton growth (Falkowski, 1994; Basu and
101 Mackey, 2018). For instance, the addition of Fe is well known to stimulate phytoplankton blooms in those vast ocean
102 regions where Fe levels limit growth (Boyd et al., 2007; Moore et al., 2013). However, some trace metals can also inhibit
103 phytoplankton growth, and different phytoplankton species have different requirements and tolerances for trace metals
104 (Sunda, 2012) so the addition of trace metals via OAE may change phytoplankton community composition.

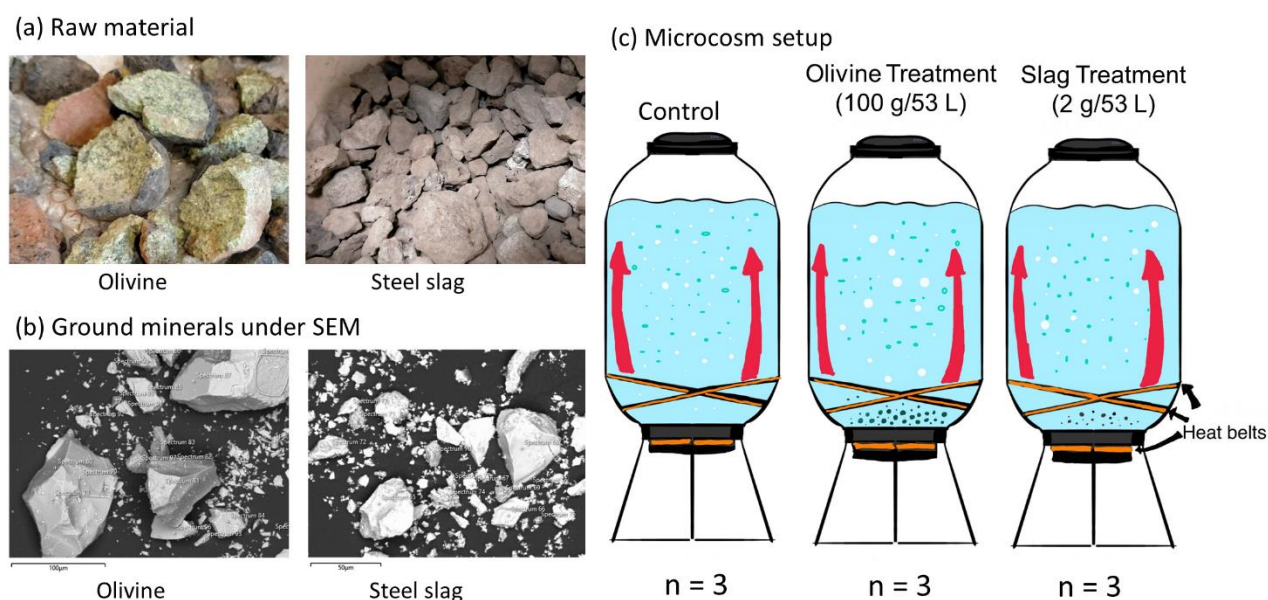
105

106 Here, we describe a microcosm experiment with coastal Tasmanian plankton communities that was used to investigate: (1)
107 how effectively OAE via the application of finely ground olivine and steel slag could sequester atmospheric CO₂, and (2)
108 if /how olivine and steel slag additions affect various components of the plankton community.

109

110 2 Methodology

111 2.1 Microcosm setup



112

113 **Fig. 1.** Experimental design and alkalinity sources. (a) Raw materials used as alkalinity sources: olivine (left) and steel-slag (right).
114 Olivine and steel-slag were originally larger than 20 mm. (b) Ground minerals observed with a scanning electron microscope (SEM).
115 (c) Microcosm setup: each microcosm enclosed ~ 53 L of surface seawater with natural plankton communities. Olivine and steel-slag
116 treatments and the control were kept in a temperature-controlled room and two heat belts were attached to the bottom of each microcosm
117 to create convective circulation.

118

119 We used nine 53 L transparent Kegland® Fermzilla conical unitank fermenters (polyethylene terephthalate) (Fig. 1) as
120 microcosms to incubate natural plankton communities. All microcosms were prewashed with hydrochloric acid (10 % v/v)
121 and rinsed five times with 18.2 MΩ Milli-Q water. Seawater with coastal plankton communities was collected at Battery
122 Point, Tasmania (42.892°S, 147.337°E) within 2 hours by lowering the microcosms into the ocean with a crane and filling
123 them in a manner similar to a Niskin bottle, as described in detail in Ferderer et al. (2022). A sieve with a mesh size of 2
124 mm was attached to the top and bottom of the microcosms during filling to avoid the entrapment of large and patchily
125 distributed organisms in the microcosms. The enclosed seawater weight was initially between 52.35-54.70 kg. After
126 seawater collection, filled microcosms were immediately transported back to the Institute for Marine and Antarctic Studies
127 (University of Tasmania) on a truck and transferred within 75 min into a temperature-controlled room set to 7.5-8 °C. Two
128 heat belts were attached to the bottom of each microcosm to induce a convective mixing current (Ferderer et al., 2022).
129 Seawater temperature inside the microcosms was about 13.5 °C due to the heating effects of the heat belts and was the
130 same as the sampled region. LED light strips were used to provide an average light intensity of 236 $\mu\text{mol photons m}^{-2} \text{s}^{-1}$
131 (ranging from 208 to 267 $\mu\text{mol photons m}^{-2} \text{s}^{-1}$) with a daily light-dark cycle of 10:14 hours. The light intensity was the
132 average light intensity in each microcosm measured with a LICOR light meter at 0.15 m depth within the microcosm.
133 Microcosms positioned in the temperature-controlled room were shuffled anti-clockwise every day to ensure similar light

134 intensity for each microcosm throughout the experiment. Treatments were established 24 hours after collecting the seawater.
135 The total alkalinity released per amount of mineral powder added was much higher for the slag powder than the olivine
136 powder in our preliminary test trials. So, three microcosms were enriched with 100 g of olivine powder, three microcosms
137 with 2 g of steel slag powder, while the remaining three microcosms were left unperturbed and served as controls.

138

139

140 **2.2 Preparation of olivine and steel slag powder**

141 The olivine rocks were provided by Moyne Shire Council who sourced the mineral from a quarry in Mortlake, Victoria,
142 Australia. The Basic Oxygen Slag (hereafter referred to as “slag”) was provided by Bradley Mansell who sourced the
143 material from Liberty Primary Steel Whyalla Steelworks in Whyalla, South Australia, Australia. Upon delivery, the olivine
144 rocks were 40-80 mm in diameter, and slag aggregates were 20-50 mm in diameter. These were crushed to smaller than 10
145 mm pieces using a hydraulic crusher. The crushed material was further ground with a ring mill with a chrome milling pot.
146 Afterwards, finely-ground samples were sieved to get samples with 150 ~ 250 μm grain size. The sieved olivine and slag
147 grains were inspected for their appearance and elemental composition using a Hitachi SU-70 analytical field emission
148 scanning electron microscope (SEM), and energy dispersive spectrometers (Central Science Laboratory (CSL), University
149 of Tasmania). Grain size spectra were determined with a Sympatec QICPIC particle size analyser LIXCELL (CSL,
150 University of Tasmania).

151

152 **2.3 Seawater sampling**

153 Seawater was transferred with a peristaltic pump from the microcosms at a depth of about 0.15 m into 1 L acid-washed
154 sampling bottles (LDPE) using an acid-washed silicon tube. Seawater in these bottles was then subsampled for dissolved
155 trace metal samples, filtrations, Fast Repetition Rate fluorometry (FRRf), and flow cytometry analysis. Samples for
156 nutrients and total alkalinity (TA) were transferred using the same pump but through a silicone tube into 80 mL HDPE
157 bottles. Total alkalinity and macronutrient samples were filtered during this process through a 0.2 μm nylon filter attached
158 to the silicone tube to remove all particles and organisms $> 0.2 \mu\text{m}$.

159

160 **2.4 Salinity, nutrients, carbonate chemistry, and trace metal analysis**

161 Salinity was measured before and at the end of the experiment using a HACH HQ40d portable meter. The pH_T (total scale)
162 and temperatures were measured daily (2-3 hours after the onset of the light period) using a pH meter (914
163 pH/Conductometer Metrohm). We recorded voltages and temperature from the pH meter and calibrated the pH_T at original
164 temperature at sampled time using the certified reference material (CRM) Tris buffer following the method described in
165 SOP6a by Dickson et al. (2007). Briefly, the standard buffer’s pH and voltage at different temperature gradients were
166 recorded, and temperature vs. voltage polynomial regression data were generated for calculating calibrated pH values (pH_T)
167 (refer to Eq. 3 in SOP6a of Dickson et al. (2007)). The regression could then be used to obtain a CRM pH value for each
168 temperature and to calibrate the pH measured in the microcosms to the total pH scale.

169

170 Total alkalinity was sampled every four days. It was measured in duplicate using a Metrohm 862 Compact Titrosampler
171 coupled with an Aquatrode Plus with PT1000 temperature sensor following the SOP3b open-cell titration protocol
172 described in Dickson et al. (2007). Filtered TA samples were stored at 8 °C for a maximum of 23 days before measurement.
173 Titration curves were evaluated using the “calculate” script within PyCO2sys by Humphreys et al. (2022). The carbon
174 chemistry equilibrium was calculated with the R package “seacarb” Gattuso et al. (2023) from pH_T , TA, phosphate, silicate,
175 temperature, and salinities using stoichiometric equilibrium constants from Lueker et al. (2000). Dissolved macronutrients
176 were measured every second day using standard spectrophotometric methods developed by Hansen and Koroleff (1999)
177 on the day the samples were taken from the microcosms.

178
179 Dissolved trace metal concentrations were measured four times during the experiment: a few hours before olivine and slag
180 were added, a few hours after these minerals were added on day 2, near the middle of the experiment on day 13, and at the
181 end of the experiment on day 22. Sixty mL of seawater was collected using an acid-washed 60 mL syringe, and the seawater
182 was filtered through 25 mm diameter 0.2 μm pore size polycarbonate filters. Unfortunately, we did not notice that 0.2 μm
183 pore size nylon filters (acid washed) were used during sampling on days 1 and 2 so we refiltered these seawater samples
184 again using 0.2 μm pore size polycarbonate filters after one month. All seawater samples were diluted approximately 20-
185 fold by weight using Milli-Q water (18.2 $\text{M}\Omega\cdot\text{cm}$ grade) and acidified using 1 % ultrapure HCl. These samples were
186 analysed using Sector Field Inductively Coupled Plasma Mass Spectrometry (SF-ICP-MS) employing multiple resolution
187 settings to overcome major spectral interferences. Due to the presence of abundant major metal ions in our samples, such
188 as Na and Mg, natural open-ocean seawater from the Southern Ocean with very low trace metal concentrations was diluted
189 20 times with Milli-Q water ~~water~~ and used as a representative blank. The same Southern Ocean seawater was enriched
190 with different gradients of trace metal standards to calculate the samples’ trace metal concentrations. ~~Seven-Five~~ of the
191 total 36 samples had abnormal trace metal ~~or phosphate~~ concentrations, and 24 of them were from day 1. We considered
192 ~~them-values~~ as outliers contaminated using the interquartile range (IQR) criterion on pre-addition data, and if values are
193 more than 10 times higher than replicates, they are also considered as outliers. These samples containing outliers were
194 excluded ~~them~~ from the data analysis (Table S1.). The major likely source of these metal contaminations is sampling in the
195 temperature control room, where precautions were insufficiently implemented.

196

197 **2.5 Particulate matter and plankton community analysis**

198 Chlorophyll *a* was sampled every second day by filtering the seawater through glass fibre filters (GF/F, pore size = 0.7 μm ,
199 diameter = 25 mm), and filters were stored in 15 mL polypropylene tubes wrapped with aluminium foil and stored at -80 °C
200 for 50-70 days before measurement. Each filter was immersed in 10 mL 100 % methanol for 18-20 h to extract chlorophyll
201 from phytoplankton and these samples were analysed on a Turner fluorometer (Model 10-AU) following the method
202 described by Evans et al. (1987).

203

204 Phytoplankton flow cytometry samples were fixed with 40 μL of a mixture of formaldehyde-hexamine (18 %:10 % v/w)
205 added to 1400 μL of seawater sample. All bacteria samples (700 μL) were fixed with 14 μL glutaraldehyde (Electron-
206 microscope grade, 25 %). After mixing samples with fixatives, samples were stored for 25 minutes at 10 °C, then flash-
207 frozen in liquid nitrogen, and stored at -80 °C until measurement 83-86 days later. Directly before the measurement,
208 samples were thawed at 37 °C. Bacteria samples were stained with SYBR green I (diluted in dimethylsulfoxide) at a final

209 ratio of 1:10000 (SYBR Green I: sample).

210

211 A Cytex Aurora flow cytometer (Cytex Biosciences) was used to quantify the abundance of fluorescing particles such as
212 phytoplankton or stained bacteria. Phytoplankton groups were distinguished based on their fluorescence signal intensity of
213 different laser excitation/emission wavelength combinations and forward scatter (FSC). The yellow-green laser (centre
214 wavelength: 577 nm), in combination with FSC signal strength, was used to separate cyanobacteria and cryptophytes from
215 other phytoplankton. The violet laser (centre wavelength: 664 nm) in combination with FSC was used to distinguish
216 picoeukaryotes, nanoeukaryotes, and microphytoplankton. The blue laser (centre wavelength: 508 nm) in combination with
217 FSC was used to distinguish bacteria from other living (i.e., DNA-containing) particles (Fig. S. 1).

218

219 The biovolume of each classified flow cytometry phytoplankton type was calculated using the equation:

220

$$221 \text{ Biovolume} = \text{Cell number count} \times \left(\frac{\text{FSC}}{10248}\right)^{2.14} \quad (4)$$

222

223 Where biovolume is the biovolume of the phytoplankton (μm^3), cell number is the cell count per mL of sample, and the
224 FSC is the forward scatter signal value from the flow cytometry. This equation is calculated based on the relationship
225 between biovolume and FSC for different phytoplankton species (Selfe, 2022). [The biovolume of each phytoplankton type](#)
226 [was then divided by the total biovolume of all phytoplankton type to calculate the biovolume proportion of each](#)
227 [phytoplankton type \(Biovolume prop.\). This derived value was used to estimate the phytoplankton composition in each](#)
228 [microcosm.](#)

229

230 Phytoplankton photosynthetic performance was estimated from the rapid light curves measured with an FRRf (FastOcean
231 Sensor FRRf3, Chelsea Instruments Group) every second day following the protocol adapted from Schallenberg et al.
232 (2020). Samples were kept in the dark for 20 minutes before the measurement and then added to the FRR fluorometry
233 cuvette, which was temperature-controlled at 13.5 °C. Filtered natural seawater was used for blank correction. The A
234 channel with [different three](#) light wavelengths (450, 530, and 624 nm) was used in each acquisition sequence. At least 10
235 acquisitions were measured for each sample. The maximum electron transport rate (ETR_{max}), initial slope of the rapid light
236 curve (α), and the light-saturation parameter (E_k) were calculated using the equation described by Platt et al. (1980) without
237 photoinhibition:

238

$$239 \text{ ETR} = \text{ETR}_{\text{max}} \left[1 - e^{-\frac{\alpha E}{\text{ETR}_{\text{max}}}}\right] \quad (5)$$

240

241 These parameters together with the maximum quantum yield of PSII (F_v/F_m) were used to compare the photosynthetic
242 performance of the phytoplankton communities in different microcosms.

243

244 Seawater was sampled before the treatment and at the end of the experiment for particulate trace metal concentrations.
245 Samples of 100 mL were filtered through an acid-cleaned polycarbonate filter (25 mm diameter, 0.8 μm pore size) and
246 placed in an acid-cleaned polypropylene filter holder ~~on~~ in a trace metal-clean laminar flow bench. The filters were washed
247 with the EDTA-oxalate reagent (1.4 mL) twice (8 min total) and rinsed with chelexed NaCl solution (0.6 mol L⁻¹ with 2.38
248 mmol L⁻¹ of HCO₃⁻, pH=8.2) 10 times (1.5 mL aliquots) (Tovar-Sanchez et al., 2003; Tang and Morel, 2006). Filters were

249 stored in acid-washed well plates at -20 °C before analysis. The digestion process followed the method reported by Bowie
250 et al. (2010). Briefly, all samples and triplicate certified reference materials plankton standards (50 mg/vial) were digested
251 in a mixture of strong ultrapure acids (750 µL 12 mol L⁻¹ HCl, 250 µL 40 % HF, 250 µL 14 mol L⁻¹ HNO₃) in 15 mL Teflon
252 perfluoroalkoxy (PFA) vials on a 95 °C hot plate for 12 h in a fume hood. They were then dry evaporated for 4 h and re-
253 suspended in 10 % v-v ultrapure HNO₃. All prepared solutions had indium as internal standard added to a final
254 concentration of 10 µg L⁻¹. Three pre-mixed multi-element standard solutions (MISA) were prepared as external calibration
255 standards.

256

257 Particulate organic carbon (POC) was sampled by filtering 100 mL of seawater from each microcosm. Glass fibre filters
258 (Whatman GF/F, pore size =0.7 µm, diameter =13 mm) were pre-combusted at 400 °C for 6 h. Filters were stored at -20 °C
259 before measurement. Samples were treated via fuming with 2N HCl to remove carbonates overnight and dried in the oven
260 for 4h. Finally, filters were folded into silver cups and stored in a desiccator until analysis. Samples were analysed for
261 carbon with a Thermo Finnigan EA 1112 Series Flash Elemental Analyser (CSL, University of Tasmania).

262

263 Biogenic silica (BSi) concentrations were analysed every 4 days by filtering 100 mL of seawater from each microcosm.
264 Mixed Cellulose Ester (MCE) membrane filters (diameter = 25 mm, pore size = 0.8 µm) were used for BSi samples. BSi
265 filters were placed in a plastic petri dish and stored at -20 °C before measurement. Filters were processed using the hot
266 NaOH digestion method of Nelson et al. (1989). The final solution was measured using the same process as the dissolved
267 silicate (see section 2.4).

268

269 A self-made plastic zooplankton net (20 mm height and 15 mm width) with a 210 µm mesh size was acid-washed first and
270 then used to collect zooplankton from microcosms before mineral addition on day 2, near the middle (day 13), and at the
271 end of the experiment (day 23). Samples were stored in 10 % formalin seawater solutions and kept at room temperature
272 until measurements. Zooplankton were quantified and identified under a Leica M165C microscope fitted with a Canon 5D
273 camera. The number of zooplankton from one mini-trawl in each collection was converted to the unit of individual L⁻¹ and
274 used for data analysis. The diversity of zooplankton communities was estimated with the Shannon Diversity Index (H)
275 calculated as:

276

$$277 \quad H = -\sum(pi \times \ln(pi)) \quad (6)$$

278

279 where pi is the proportion of the entire zooplankton community made up of individual species abundance, and ln is the
280 natural logarithm.

281

282

283 **2.6 Statistic analysis**

284 R studio was used for data analyses. Generalized additive models (GAMs) from the package “mgcv” were fitted to the data
285 to predict the changes over time. The GAMs all shared the same equations:

286

$$287 \quad Y = s(Day), \quad (7)$$

288

289 in which Y presents the dependent variable and $s(\text{Day})$ is the smooth term of the day of the experiment. Another GAM was
290 used to detect significant differences between treatments and the control:

291

$$292 \quad Y = \textit{Treatment} + s(\textit{Day}) + s(\textit{Day}, \textit{by} = \textit{oTreatment}) \quad (8)$$

293

294 In this equation, the variable “Treatment” includes three conditions: “Control”, “Slag” and “Olivine”; while “oTreatment”
295 is the ordered factor of the variable “Treatment” which allowed us to compare the GAMs smooth terms from different
296 treatments and the control (Simpson, 2017).

297

298 When comparing GAMs, P-means represent the p-value obtained from comparing two GAMs, such as the control and the
299 olivine treatment. If P-means is below 0.05, it indicates that the mean values of the two GAMs exhibit significant
300 differences over the course of the experiment. Conversely, if P-means is equal to or greater than 0.05, it suggests that the
301 two GAMs have similar mean values. In contrast, P-smooths represents the p-value derived from comparing the smooth
302 terms of two GAMs. If P-smooths is below 0.05, it indicates that the two GAMs demonstrate significantly different trends
303 in their change over time.

304

305 For the analysis of trace metal concentrations and zooplankton abundance, Generalized Linear Models (GLMs) from the
306 'stats' package were fitted to the data to determine significant differences between treatments and the control. The selection
307 of specific GLMs was based on the distribution of the raw data. One GLM equation is

308

$$309 \quad Y = \textit{Treatment} + \frac{\textit{Day}}{22} + \left(\frac{\textit{Day}}{22}\right)^2 \quad (9)$$

310

311 with family = Gamma, where Y represents the measured parameter (abundance of a zooplankton species and dissolved
312 trace metal concentrations); treatment is the conditions (“Control”, “Slag” and “Olivine”); and Day represents the day of
313 the experiment. The other GLM equation,

314

$$315 \quad Y = \textit{Treatment} + \textit{Day} \quad (10)$$

316

317 with family = Gaussian, was employed for particulate trace metal data and the Shannon Diversity Index. To compare the
318 contribution of the three treatments on the measured parameters, Tukey's significant difference test was conducted on the
319 GLMs using the 'glht' function.

320

321 **3. Results**

322 **3.1 Elemental composition and grain size of the finely-ground minerals**

323 SEM analysis revealed the approximate elemental composition of olivine and slag powder (Table 1). Based on this analysis
324 the olivine composition resembles the Mg-rich olivine mineral “forsterite” (Mg_2SiO_4). The particle size spectrum of olivine

325 powder is shown in detail in Fig. S2. Roughly 69 % of the olivine particles, when measured by volume, fell within the
 326 diameter range of 35 - 300 μm . Additionally, SEM analysis revealed high levels of Ca and O in the slag, indicative of the
 327 considerable $\text{Ca}(\text{OH})_2$ and CaO content of the powder (Table 1; please note that H cannot be measured with the applied
 328 method). The particle size measurement (Fig. S2) showed that 78 % of the ground slag particles were between 35 - 300
 329 μm .

330

331 **Table 1.** The weight percentage of elements from two minerals. Unit: wt %.

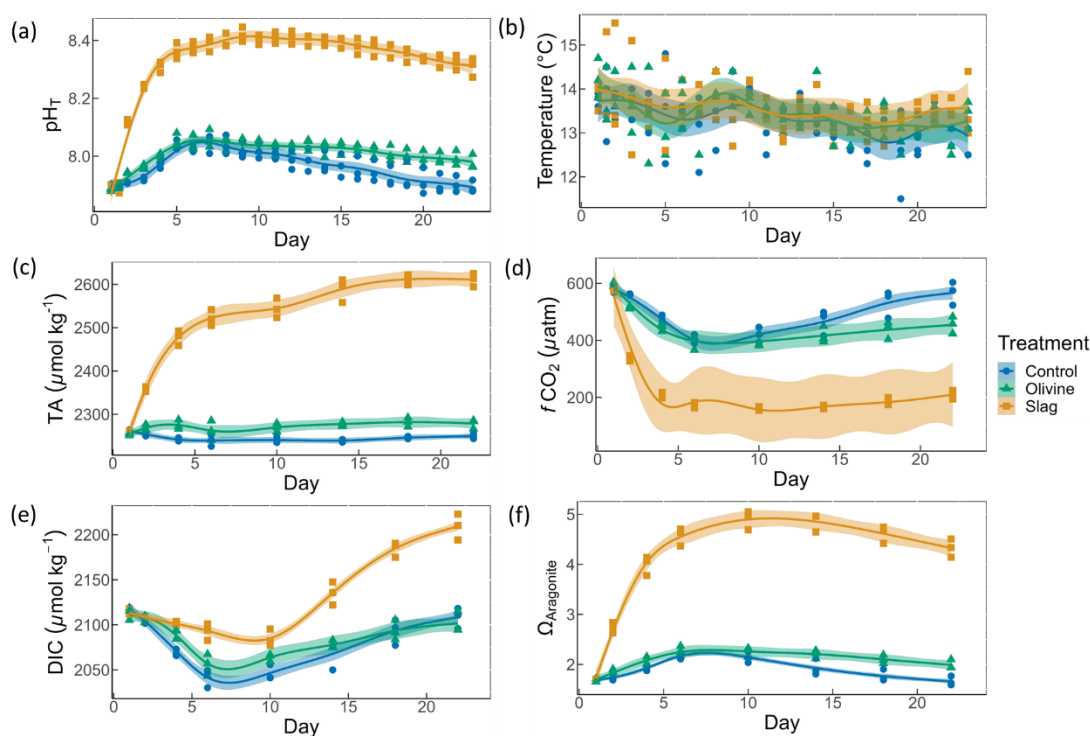
Element	O	Ca	Mn	Si	Mg	Fe	Al	Ti	Cr	Ni
Olivine	39.9	0.4		19.9	26.4	13.0	1.0			0.8
Steel slag	41.9	36.0	7.0	6.5	4.3	3.7	3.4	1.7	1.6	

332

333

334 3.2 Physical and chemical conditions over the course of the experiment.

335 On day 2 of the experiment, when olivine particles were introduced into the microcosms, the smallest fraction of the powder
 336 remained suspended, causing the seawater to become highly turbid for several days. The resulting milky appearance of the
 337 seawater eventually faded over a period of approximately five days, and by day 5, the turbidity had visually become like
 338 the slag treatment and the control. This effect was not anticipated, and as a result, we decided to investigate its impact on
 339 light intensity. To do so, a test was conducted after the main experiment in which olivine powder was added to a microcosm
 340 identical to those used in the experiment, and light intensity was measured daily at a depth of 0.15 m. The results showed
 341 that the addition of olivine caused an initial reduction in light intensity of 18.5 % at 15 mins after addition, which declined
 342 to 7.4 %, 3.7 %, 3.7 % and 0 % after 1, 2, 3, and 4 days, respectively. These findings indicate that olivine additions can
 343 significantly affect the light environment in the microcosms, whereas no such effect was observed in the slag treatment.
 344



345

346 **Fig. 2.** Carbonate chemistry conditions. The temporal development of (a) pH_T, (b) temperature, (c) total alkalinity (TA), (d) CO₂ fugacity
347 (*f*CO₂) computed at *in situ* temperature and atmospheric pressure, (e) dissolved inorganic carbon (DIC), and (f) aragonite saturation state
348 ($\Omega_{\text{aragonite}}$). The dots represent the raw data (n=3 for each treatment per sampling time), and the fitted curve is the generalized additive
349 model (GAM). The shading represents the 95 % confidence interval of the fitted GAM.

350

351 The pH_T of all microcosms increased ~~to various extents~~ from day 1 to day 5 (Fig. 2a). This was ~~partially~~ due to
352 photosynthetic CO₂ drawdown ~~in the control or photosynthetic CO₂ drawdown in combination with alkalinity release from~~
353 ~~minerals in the treatments.~~ During the peak of the bloom, ~~olivine addition led to a slightly higher~~ pH_T ~~was~~ 8.037 ± 0.010
354 ~~in the control~~ (8.054 ± 0.014 , (average values \pm standard error), 8.054 ± 0.014 ~~-in the olivine treatment and-~~ 8.411 ± 0.015
355 ~~in the slag treatment.~~ The- pH_T was significantly higher ~~in the slag~~ than the olivine treatment and the control throughout
356 the experiment (~~control and olivine pH_T were not significantly different~~). The final pH_T of the control, olivine, and slag
357 treatments were 7.893 ± 0.012 , 7.978 ± 0.015 , and 8.309 ± 0.019 , respectively. ~~The temperature inside of the microcosms~~
358 ~~varied-in between replicates, which may have added noise in the biological response data.~~ However, on average there was
359 ~~no statistically significant difference between control/treatments during the experiment.~~

360

361 ~~When comparing GAMs, P means represent the p value obtained from comparing two GAMs, such as the control and the~~
362 ~~olivine treatment. If P means is below 0.05, it indicates that the mean values of the two GAMs exhibit significant~~
363 ~~differences over the course of the experiment. Conversely, if P means is equal to or greater than 0.05, it suggests that the~~
364 ~~two GAMs have similar mean values. In contrast, P-smooths represents the p value derived from comparing the smooth~~
365 ~~terms of two GAMs. If P-smooths is below 0.05, it indicates that the two GAMs demonstrate significantly different trends~~
366 ~~in their change over time.~~ In our ~~data~~ analysis, all the fitted GAMs from the treatments and the control exhibited significant
367 differences in pH_T from each other, as evidenced by the p-values of both P-means and P-smooths being smaller than 0.001.
368 For detailed results of the GAM p-values, please refer to Table S2~~4~~.

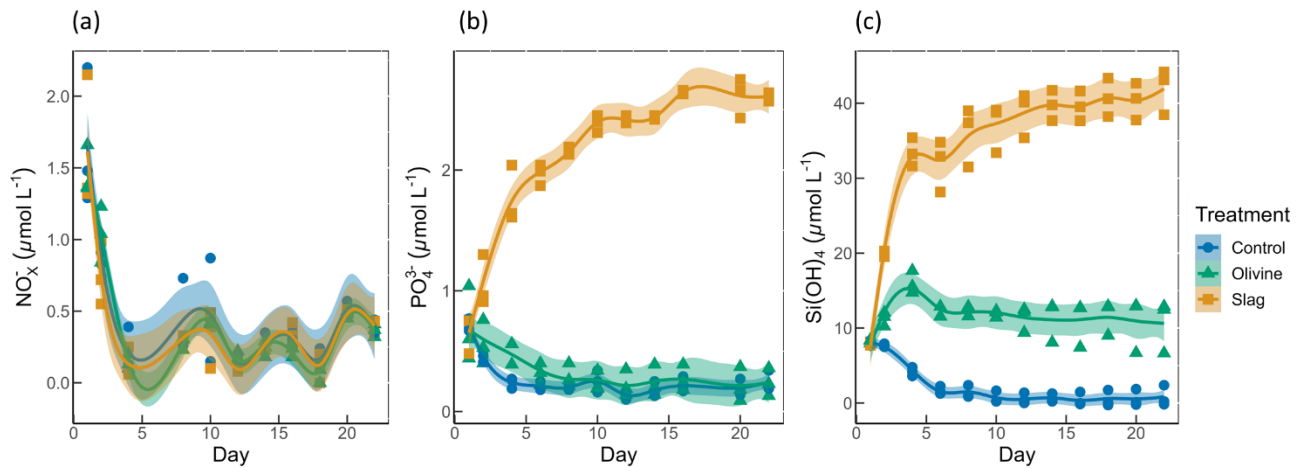
369

370 Total alkalinity increased marginally from 2255 ± 2 to 2262 ± 13 $\mu\text{mol kg}^{-1}$ within the first 6 days after olivine addition
371 while it increased more substantially from 2259 ± 1 to 2522 ± 11 $\mu\text{mol kg}^{-1}$ in the same time span in the slag treatment (Fig.
372 2c). The TA in the control decreased from 2261 ± 2 $\mu\text{mol kg}^{-1}$ to 2240 ± 7 $\mu\text{mol kg}^{-1}$ from day 1 to day 6 but remained
373 stable thereafter. The TA reached 2279 ± 6 $\mu\text{mol kg}^{-1}$ in the olivine treatment and 2611 ± 9 $\mu\text{mol kg}^{-1}$ in the slag treatment
374 ~~group~~ on day 22. The slag treatment reached a significantly higher TA than the olivine treatment and the control (P-smooths
375 < 0.001). The mean TA from GAM in olivine treatment was higher than the control ~~group~~ (P-means < 0.001).

376

377 The CO₂ fugacity (*f*CO₂) computed at *in situ* temperature and atmospheric pressure decreased continuously in the first 6
378 days in all microcosms (Fig. 2d). Then it increased again in the control and olivine treatments while staying lower in the
379 slag treatment (P-means and P-smooths < 0.001 between either treatment or the control). Dissolved inorganic carbon (Fig.
380 2e) and the aragonite saturation state ($\Omega_{\text{aragonite}}$; Fig. 2f) revealed a similar trend over the course of the experiment in the
381 control and the olivine treatment. In contrast, the slag treatment had higher DIC and $\Omega_{\text{aragonite}}$ values throughout the
382 experiment (P-means < 0.001).

383



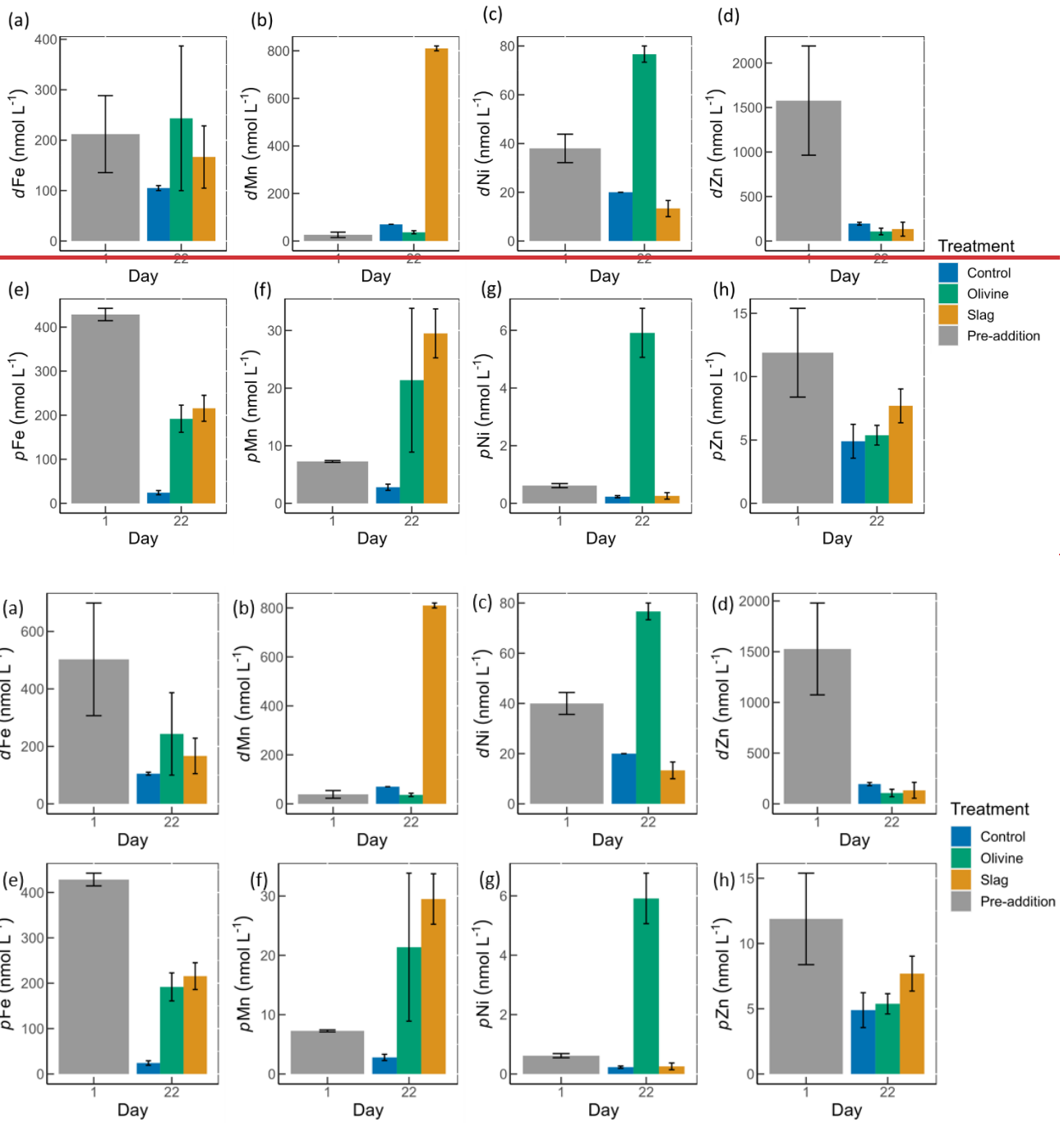
384

385 **Fig. 3.** Macronutrients concentrations over the course of the study. (a) Nitrate and nitrite concentrations. (b) Phosphate concentrations.
 386 (c) Silicic acid concentrations. The dots represent the raw data ($n=3$ for each treatment per collection), and the fitted curve is the
 387 generalized additive model.

388

389 Initial nitrate and nitrite (NO_x^-), phosphate (PO_4^{3-}), and silicic acid (Si(OH)_4) concentrations were 1.58 ± 0.12 , 0.69 ± 0.59 ,
 390 and $8.04 \pm 0.10 \mu\text{mol L}^{-1}$, respectively (Fig. 3). NO_x^- declined rapidly in all microcosms once the experiment had
 391 commenced to values below $0.5 \mu\text{mol L}^{-1}$ and no significant difference was detected between treatments and control (P -
 392 smooths >0.05 ; Fig. 3a). In both the olivine treatment and the control, the PO_4^{3-} concentration decreased in the first six
 393 days (Fig. 3b). In the slag treatment, PO_4^{3-} increased to a maximum of $2.65 \pm 0.01 \mu\text{mol L}^{-1}$, which was significantly higher
 394 than in the olivine treatment and the control (P -means <0.001). The Si(OH)_4 concentration increased to a maximum of
 395 $15.99 \pm 0.87 \mu\text{mol L}^{-1}$ in the olivine treatment, increased to a maximum of $41.92 \pm 1.75 \mu\text{mol L}^{-1}$ in the slag treatment, but
 396 decreased below the detection limit in the control (Fig. 3c). Significant differences were observed in the development of
 397 Si(OH)_4 between all treatments and the control (Table S2+).

398



399

400

401

402 **Fig. 4.** Dissolved and particulate trace metal concentrations in microcosm seawater. (a)-(d) are dissolved trace metal concentrations, and
 403 (e)-(h) are total particulate trace metal concentrations. The error bars represent the standard error from measured samples. The pre-
 404 addition data shown in (a)-(d) represent the average of 75 microcosms before addition of slag or olivine. The data for the control on day
 405 22 in (a)-(d) and for the pre-addition on day 1 in (e)-(h) were based on two of three microcosm replicates. The remaining data were based
 406 on all three microcosm replicates.

407

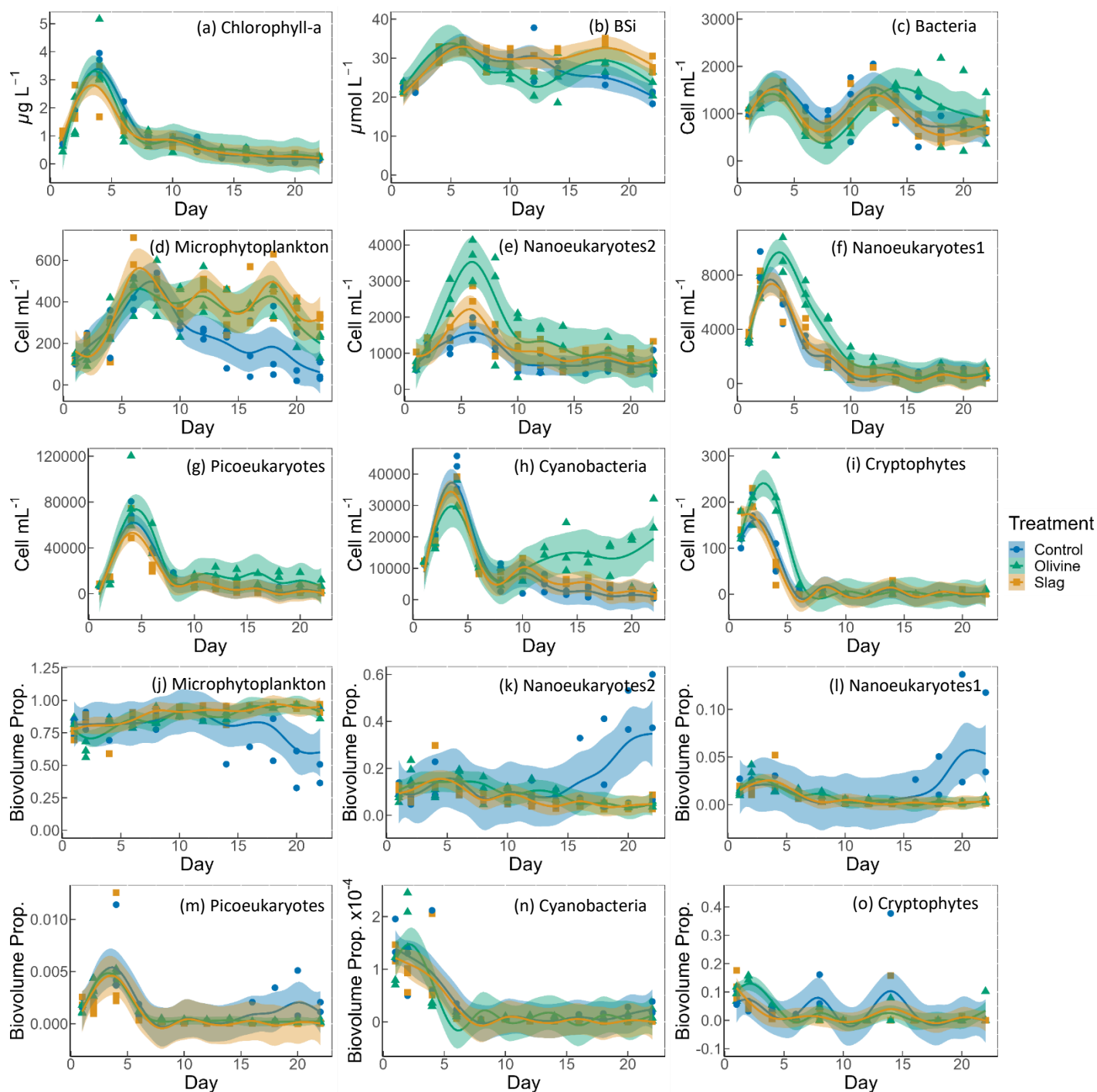
408 The dissolved trace metal concentrations measured from microcosms are presented in Fig. S3. While the mass of olivine
 409 added to the microcosms was 50-fold greater (100 g vs 2 g), it's noteworthy that the variation in dissolved trace metal

410 ~~concentrations between the two treatments were much smaller than 50 folds.~~ After 21 days of experiment, the treatments
411 showed an ~~significant~~ increase in dissolved Al concentrations from ~~504-920 ± 28680~~ to $970 \pm 228 \text{ nmol L}^{-1}$ in olivine
412 treatment, and from ~~504-920 ± 28680~~ to $1093 \pm 77 \text{ nmol L}^{-1}$ in slag treatment, while in the control dissolved Al decreased
413 to $230 \pm 10 \text{ nmol L}^{-1}$ (Fig. S3). The fitted GLMs were compared, and the p-value revealed how much influence a treatment
414 had on the dissolved metal concentrations (Table S32). The results indicate that the slag and olivine additions led to
415 significantly higher Al concentrations than in the control (p-values < 0.05), but no significant difference was found between
416 the two treatments (p-value = 0.189). ~~The olivine treatment released Cu into the seawater, and t~~The Cu concentration in
417 the olivine on day 22 was significantly higher than the slag treatment and the control (p-value < 0.05) (Fig. S3). The addition
418 of olivine and slag released some dissolved Fe, but overall, the concentration of Fe did not differ significantly between
419 treatments (Fig. 4a, Table S3). The slag released a substantial amount of dissolved Mn (maximum ~~8120 ± 10 nmol L⁻¹~~ on
420 day 22) (Fig. 4b), leading to significantly higher concentrations than in the olivine treatment and the control (p-values <
421 0.001). A significant amount of dissolved Ni (maximum $77 \pm 3 \text{ nmol L}^{-1}$ on day 22) was released from the olivine powder
422 (p-values < 0.001) (Fig. 4c). The initial concentration of dissolved Zn in seawater was much higher than on day 22 in all
423 microcosms, and no significant difference in Zn concentrations was found between the treatments and the control.

424
425 Particulate concentrations of some trace metals also differed between treatments. The total particulate Fe decreased in all
426 microcosms on day 22 comparing with the pre-addition level, but both mineral addition treatments had higher particulate
427 Fe concentrations than the control (Fig. 4e). The addition of slag elevated particulate Mn concentrations to a level higher
428 than the pre-addition and the control on day 22 (Fig. 4f), while the addition of olivine increased the particulate Ni
429 concentrations to a level higher than the slag, the control, and the pre-addition (Fig. 4g). The particulate Zn concentrations
430 in general decreased by the end of the experiment (Fig. 4h), and no significant differences were found between the
431 treatments and the control.

432
433 The POC on day 1 and day 22 from all microcosms were very similar, 10.99 ± 0.58 and $11.03 \pm 0.41 \text{ } \mu\text{mol L}^{-1}$ respectively
434 (Fig. S4) so the metal:POC results were consistent with the particulate trace metal results (Fig. 4 e-h). In general, the non-
435 surface metal:POC are positively correlated with the total metal:POC ratios (Fig. S5). The ratio of non-surface to total
436 particulate trace metal concentrations is summarized in Table S54. Both non-surface and total Fe concentrations decreased
437 in microcosms on day 22 compared with the pre-addition level. Iron:POC ratios were significantly higher in the treatments
438 than in the control on day 22 (p-values < 0.05, Table S32), and there was no significant difference between mineral addition
439 treatments. The non-surface to total Fe:POC ratios were > 0.94 in all microcosms on both day 1 and day 22. The total and
440 non-surface Mn:POC ratio was the highest in the slag treatment. These ratios were higher than the pre-addition level and
441 the control at the end of the experiment. The total particulate Ni concentrations in the olivine treatment were significantly
442 higher than before olivine addition. The olivine treatment led to a >22-fold higher Ni:POC ratio compared to the other two
443 treatments (p-value < 0.001).

444
445
446



448
 449 **Fig. 5.** Temporal development of chlorophyll-a concentration (chl-a), BSi, and different eukaryotic and bacterial plankton groups as
 450 determined with flow cytometry. (a) chlorophyll-a; (b) BSi; cell concentrations of (c) heterotrophic bacteria, (d) microphytoplankton, (e)
 451 nanoeukaryotes2, (f) nanoeukaryotes1 (g) picoeukaryotes, (h) cyanobacteria, and (i) cryptophytes; biovolume proportion of (j)
 452 microphytoplankton, (k) nanoeukaryotes2, (l) nanoeukaryotes1 (m) picoeukaryotes, (n) cyanobacteria, and (o) cryptophytes. The figure
 453 data points represent the raw data, and the fitted curve is the generalized additive model. The shaded area represents the 95 % confidence
 454 interval.

456 The chl-a concentration in all microcosms increased from day 1 to day 4 from 1 $\mu\text{g L}^{-1}$ to 3-4 $\mu\text{g L}^{-1}$ (Fig. 5a). The chl-a
457 concentration then decreased rapidly from day 4 to day 8, then continued to decrease, though more slowly, to $<0.3 \mu\text{g L}^{-1}$
458 until the end of the experiment. The GAMs of chl-a did not show any difference between treatments and the control (both
459 P-means and P-smooths >0.05 , see Table S2+).

460

461 The BSi concentration increased from day 1 to day 6 in all microcosms (Fig. 5b). In the olivine ~~and slag~~ treatments, BSi
462 concentrations decreased slightly after the peak until day 12 but then increased again. In the slag treatment, BSi
463 concentrations remained relatively stable after the initial phytoplankton bloom. In contrast, BSi concentration decreased
464 continuously in the control after the initial peak. Olivine particles suspended in seawater after the mineral addition (see
465 section 3.2) partially ended up on BSi filters during filtration. This led to extremely high BSi measurements on days 2 and
466 4 that were removed from Fig. 5b. Without these outliers, the mean of fitted BSi GAM in the olivine treatment was lower
467 than the control and the slag treatment (Table S2+), and the slag had the highest average BSi over the course of the
468 experiment. Overall, the BSi trends in the two treatments were similar (P-smooths = 0.269), and both were significantly
469 different from the control (P-smooths <0.05).

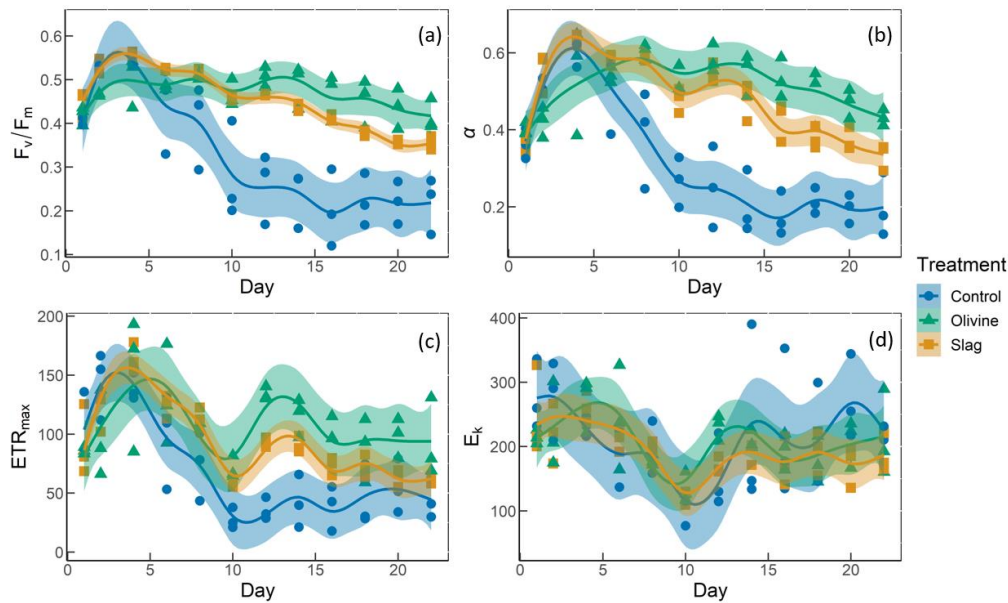
470

471 The development of the phytoplankton community composition showed significant differences between the treatments and
472 the control. In general, most phytoplankton groups exhibited similar patterns to chl-a, with peak cell numbers occurring on
473 day 4 (Fig. 5f-i) apart from microphytoplankton and nanoeukaryotes2 which had the peak delayed for 1-2 days (Fig. 5d-
474 e). Please be aware that flow cytometers may not capture some large and chain-forming phytoplankton. Following day
475 6 After reaching peak values during the bloom, phytoplankton ~~cell~~ abundance generally decreased steadily.
476 Microphytoplankton displayed similar trends to the results for BSi. Before day 10, all microcosms had similar
477 microphytoplankton abundances (Fig. 5d). However, in the control ~~group~~, microphytoplankton abundance declined
478 continuously and at a faster rate compared to the ~~other~~ two treatments (P-smooths values <0.03). From day 2 to day 6, the
479 abundance of nanoeukaryotes1, nanoeukaryotes2, picoeukaryotes, and cryptophytes was higher in the olivine treatment
480 compared to the slag treatment and the control. After day 8, their abundance in the olivine treatment decreased to a similar
481 level as the slag treatment and the control ~~other two groups~~. Notably, there were few significant differences observed
482 between the slag treatment and the control ~~group~~ in terms of the abundances of nanoeukaryotes1, nanoeukaryotes2,
483 picoeukaryotes, cyanobacteria, and cryptophytes throughout the experiment. In the olivine treatment, cyanobacteria
484 experienced a second bloom after day 10, which was significantly different from the other two groups (P-smooths <0.01).
485 Heterotrophic bacteria exhibited an increase and decline pattern following the phytoplankton bloom until day 8 (Fig. 5c).
486 Subsequently, bacteria abundance increased again, reaching a second peak during days 12-14, followed by a decline until
487 the end of the experiment. The decline in bacteria abundance was slower in the olivine treatment, although no significant
488 differences were detected between treatments (Table S2+).

489

490 Among all the microcosms, microphytoplankton, ~~nanoeukaryotes2, and cryptophytes~~ consistently accounted for the largest
491 proportion of biovolume. From the perspective of biovolume proportion, the mineral addition mainly influenced the
492 microphytoplankton and nanoeukaryotes. The control had similar phytoplankton biovolume distribution as the treatments
493 from day 1 to day 15, but after that the proportion of microphytoplankton biovolume decreased to a level significantly
494 lower than the treatments. In the control treatment, the proportion of nanoeukaryotes' biovolume increased as the proportion
495 of microphytoplankton decreased. The biovolume of picoeukaryotes, cyanobacteria and cryptophytes increased during the

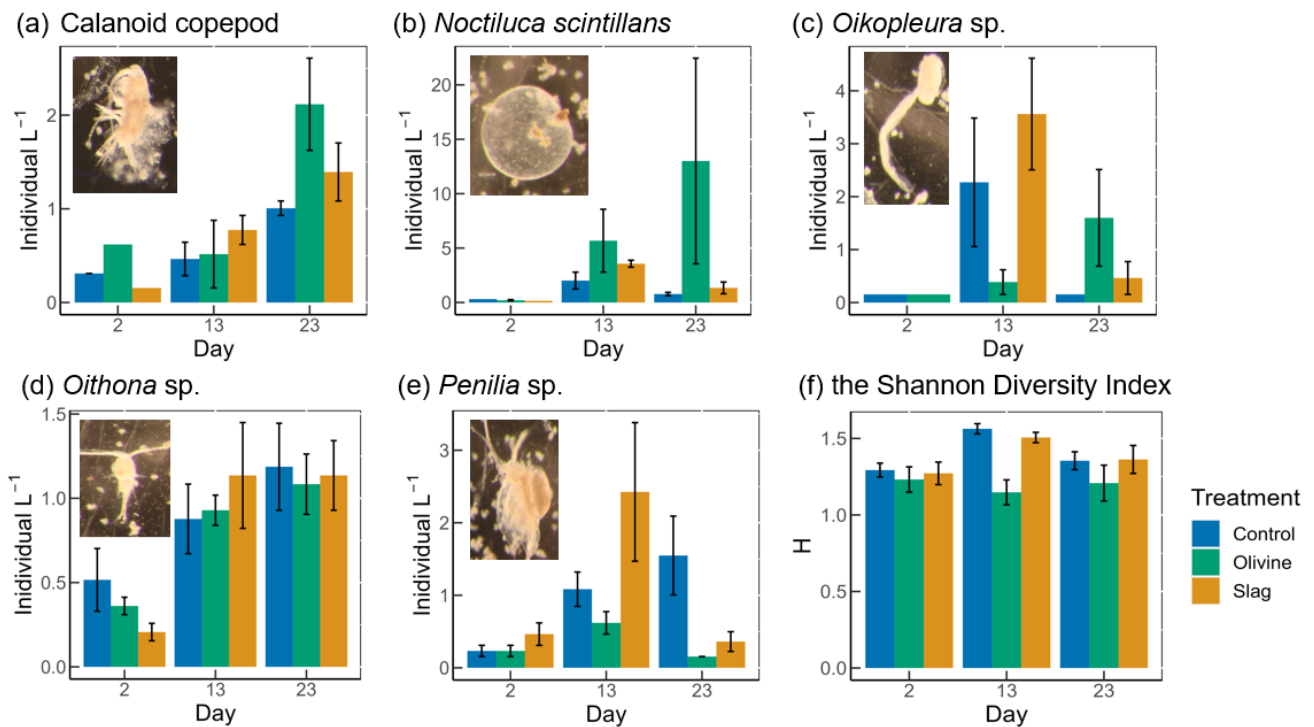
496 phytoplankton bloom and then decreased drastically after the bloom. There were no significant differences in biovolume
 497 [proportion](#) observed for picoeukaryotes, cyanobacteria and cryptophytes between the treatments and the control.
 498



499
 500 **Fig. 6.** The photosynthetic performance of the phytoplankton community. (a) F_v/F_m , the maximum quantum yield of photosynthesis II.
 501 (b) α , the initial slope of the rapid light curves. (c) ETR_{max} is the maximum electron transport rate, the maximum potential photosynthetic
 502 rate. (d) E_k is light-saturation parameter, Unit: $\mu\text{mol photons m}^{-2} \text{s}^{-1}$.

503
 504 The temporal development of F_v/F_m , α , ETR_{max} , and E_k is illustrated in Fig. 6. The F_v/F_m values of the phytoplankton
 505 community were approximately 0.42 ± 0.01 and increased to levels > 0.5 during the peak of the phytoplankton bloom on
 506 day 4 (Fig. 6a). Following the bloom, F_v/F_m values dropped below 0.3 in the control. However, the decline in F_v/F_m after
 507 the bloom was less pronounced in the two mineral addition treatments with the olivine treatment maintaining higher F_v/F_m
 508 values than the slag treatment (P-smooths < 0.05). At the end of the experiment, F_v/F_m was 0.22 ± 0.04 in the control, 0.35
 509 ± 0.01 in the slag treatment, and 0.42 ± 0.02 in the olivine treatment. The temporal development of α aligned with the
 510 patterns observed for F_v/F_m (compare Fig. 6a and 6b). The maximum values of ETR_{max} were observed on day 4 in the
 511 control and the slag treatment, while in the olivine treatment, it occurred on day 5 (Fig. 6c). Subsequently, ETR_{max}
 512 continuously decreased until day 10 and then stabilized until the end of the experiment. However, ETR_{max} exhibited a
 513 subsequent increase in the mineral treatments around day 12. The ETR_{max} values were higher in the mineral treatments
 514 compared to the control group (P-means < 0.001 , Table S2†). The parameter E_k decreased from $246 \pm 17 \mu\text{mol photons m}^{-2} \text{s}^{-1}$
 515 $\text{m}^{-2} \text{s}^{-1}$ on day 1 to $121 \pm 7 \mu\text{mol photons m}^{-2} \text{s}^{-1}$ on day 10, and then it increased again to approximately $200 \mu\text{mol photons}$
 516 $\text{m}^{-2} \text{s}^{-1}$ by the end of the experiment (Fig. 6d). The change in E_k did not exhibit significant differences between the treatments
 517 and the control (both P-means and P-smooths > 0.05).

518
 519



520

521

522

523

524

525

526

527

528

529

530

531

532

533

534

535

536

537

538

539

540

541

542

543

544

545

Fig. 7. The dominant zooplankton abundance and community diversity from different treatments. Abundance of dominant zooplankton in microcosms: (a) calanoid copepod; (b) *Noctiluca scintillans*; (c) *Oikopleura* sp.; (d) *Oithona* sp.; (e) *Penilia* sp.; and (f) the Shannon diversity index (H) of different treatments and the control. Error bars represent the standard error calculated from three microcosm replicates. Photographs of each zooplankton group are shown on the corresponding graphs.

Thirteen zooplankton taxonomic groups were identified in the microcosms. The dominant taxa were the appendicularian *Oikopleura* sp., the cyclopoid copepod *Oithona* sp., the cladoceran *Penilia* sp., the heterotrophic dinoflagellate *Noctiluca-scintillans* and several calanoid copepods including *Acartia* sp., *Paracalanus* sp. and *Gladioferens* sp. The larvae and eggs of *Oikopleura*, *Penilia* and copepod were also observed under the microscope. In general, higher zooplankton numbers were observed after the bloom on day 13 (Fig. 7). The abundance of calanoid copepods and *Oithona* sp. increased after day 2 (Fig. 7-a, d), and there was no significant difference between treatments and the control (p-values >0.05, Table S43). The abundance of *N. scintillans* increased significantly more in the olivine treatment than in the control and the slag treatment, with highest abundance of 13 ± 9 individual L^{-1} observed in the olivine treatment on the last day (Fig. 7-b). The abundance of *Oikopleura* in the control and the slag treatment was higher than the olivine treatment on day 13 but was higher in the olivine treatment on day 22 (Fig. 7c). A higher abundance of *Penilia* sp. was found in the slag treatment on day 13 and in the control on day 23 (Fig. 7e). Due to the patchy distribution of zooplankton, these data have large standard errors and only the differences in the numbers of *N. scintillans* in the olivine treatment were statistically significantly different from the slag treatment and the control (p-value <0.05, Table S43).

Considering the control and slag treatment, the Shannon Diversity Index (H) increased from day 2 to day 13 and declined on day 23, while in the olivine treatment, H was lower on day 13 than on day 2 and day 23 (Fig. 7f). The GLMs revealed that the olivine treatment had significantly lower H on day 13 than the control and the slag treatment (p-values <0.001). There were no significant differences in H between the control and the slag treatment (Table S43). The addition of olivine decreased the zooplankton community's diversity. This is mainly driven by distinct trends observed in the abundance of *Oikopleura* sp., *Penilia* sp., and *N. scintillans* (Fig. 7).

546

547 4. Discussion

548 4.1 CO₂ removal potential of slag and olivine

549 The slag powder created significantly higher CO₂ removal potential than the olivine powder over the course of the study.
550 Ca(OH)₂ and CaO in slag and Mg₂SiO₄ in olivine are likely to be the main functional minerals driving the measured
551 alkalinity enhancement. Total alkalinity increased by 361 μmol kg⁻¹ in the slag treatment while it increased by only 29
552 μmol kg⁻¹ in the olivine treatment, equivalent to a potential increase ~~of in the~~ marine inorganic carbon by 14.7 and 0.9%
553 within 3 weeks of their application. When normalizing these alkalinity increases to the same material weight, 1 g of slag
554 would release 9626 μmol TA while 1 g of olivine would release 16 μmol TA. Thus, over 3 weeks of experimental incubation,
555 slag is ~600-fold more efficient in releasing alkalinity for particles of this size class (please note that particle size spectra
556 of olivine and slag were similar but not identical; Fig. S1). We can also use these values to make a rough estimate of how
557 much CO₂ these two minerals could potentially sequester. One mole of alkalinity from olivine and slag can sequester
558 approximately 0.85 mole of CO₂. Thus, one tonne of slag and olivine powder as used here could sequester 360 and 0.6 kg,
559 respectively, within 3 weeks. It is likely that optimization of particle size and application method may lead to higher
560 efficiencies. Nevertheless, the slag showed potential as an OAE source mineral, even when applied as relatively coarse
561 powder in this experiment.

562

563 4.2 Environmental implications of slag and olivine additions

564 The amount of olivine and slag powder added to the treatments differed significantly (100 g of olivine powder were added
565 while only 2 g of slag powder were added to the 53 L microcosms). Our rationale for these different mass additions -was
566 to yield somewhat similar amounts of detectable alkalinity enhancement in the dissolved phase, since we already knew
567 from tests before the experiment that slag elevates alkalinity faster than olivine. However, olivine was less efficient in
568 releasing alkalinity than we had anticipated so that even a 50-fold higher additions of olivine (in mass) did not compensate
569 for this difference. As such, our experiments are associated with an “apples and oranges issue” in that our perturbation with
570 minerals and associated OAE differs. We argue that an adjusted addition of minerals depending on the alkalinity
571 enhancement rate would be consistent with what OAE practitioners may do under real-world conditions. Presumably, OAE
572 deployments may have to adjust the amounts of minerals to detect alkalinity enhancement in the dissolved phase for
573 verification purposes. Nevertheless, to account for the “apples and oranges issue”, the following discussion mainly relates
574 the observed environmental effects with the alkalinity enhancement achieved over the course of the study.

575 4.2.1. OAE impacts-effects on phytoplankton physiology and community

576 Previous research has hypothesised that OAE-induced changes in seawater carbonate chemistry could delay phytoplankton
577 bloom formation due to reductions in seawater pCO₂ in the aftermath of an OAE deployment (Bach et al., 2019). The build-
578 up of chlorophyll *a* concentration as observed here was indistinguishable between treatments and the control, suggesting a
579 ~~limited-no~~ effect of slag- or olivine-based OAE on phytoplankton bloom dynamics under these experimental settings. A
580 lack of bloom delay due to carbonate chemistry is unsurprising for the olivine treatment where the release of alkalinity was

581 small (29 $\mu\text{mol kg}^{-1}$ alkalinity release), but somewhat more surprising in the slag treatment where alkalinity was quite
582 rapidly increased by 361 $\mu\text{mol kg}^{-1}$. However, the release was still lower than in a very similar study by Ferderer et al.,
583 (2022) where alkalinity was increased by 500 $\mu\text{mol kg}^{-1}$ using sodium hydroxide and even there they did not observe a
584 bloom delay. Based on this very limited evidence, it seems that bloom delays do not occur consistently under OAE within
585 this alkalinity range.

586
587 The nutrient data show that the phytoplankton community was most likely N-limited after day 4 so that the release of
588 Si(OH)_4 from olivine and Si(OH)_4 and PO_4^{3-} from slag did not stimulate a further increase in chlorophyll-*a* concentration
589 in the treatments. The development of BSi concentrations is indicative of the prevalence of diatoms in the microcosms but
590 differences between treatments and the control were small. The release of Si(OH)_4 through olivine and slag will most likely
591 benefit diatoms but this fertilization effect did not manifest in this specific experiment because N was limiting diatom
592 growth. However, when new N is supplied then diatoms will likely take a bigger share of the limiting N pool when olivine
593 or slag are used for OAE, as has been shown in Si(OH)_4 manipulation experiments in and outside the context of OAE
594 research (Egge and Jacobsen, 1997; Ferderer et al., 2023). As such, diatoms are likely to benefit from olivine and slag
595 applications, ~~as has been shown in Si(OH)_4 manipulation experiments outside the context of OAE research (Egge and~~
596 ~~Jacobsen, 1997).~~ In the case of slag, the release of PO_4^{3-} will likely be another driver that affects plankton productivity and
597 community composition. As for Si(OH)_4 , however, the effect of additional PO_4^{3-} did likely not materialise in this
598 experiment because PO_4^{3-} was not limiting over the course of the study. However, in ecosystems where PO_4^{3-} is a limiting
599 resource, the application of slag could enhance productivity with associated benefits for higher trophic levels. In contrast,
600 excessive applications of slag and concomitant PO_4^{3-} release could also pose a risk of eutrophication. Future studies may
601 need to investigate what the most sustainable dose of OAE via olivine and/or slag applications could be and the suitable
602 regions for application.

603
604 The flow cytometry results further revealed the change in phytoplankton community composition. Both the olivine and
605 slag treatments sustained higher microphytoplankton abundances after the peak of the phytoplankton bloom ~~on day 6~~. This
606 trend is consistent with higher some photophysiological parameters such as F_v/F_m values in the treatments than in the
607 control so that it is tempting to assume that photophysiological fitness gain measured with the FRRf led to higher
608 competitiveness of microphytoplankton in the community. Indeed, calculations of the contribution of different
609 phytoplankton groups to total biovolume based on flow cytometry data indicate that microphytoplankton were
610 predominantly contributing to the phytoplankton community biovolume so that the responses measured by the FRRf were
611 probably to a large extent driven by this group.

612
613 Apart from the increased microphytoplankton abundance, for the slag treatment, other phytoplankton groups distinguished
614 with flow cytometry did not deviate considerably from the control. The olivine addition, however, triggered more
615 pronounced shifts in the phytoplankton community. In particular, the nanoeukaryotes (roughly between 2-20 μm),
616 picoeukaryotes and the cryptophytes showed relatively higher abundance during the peak of the phytoplankton bloom, and
617 the abundance of cyanobacteria was higher after the bloom. We speculate that this shift following olivine treatment may
618 be attributable to a top-down effect from the decrease in zooplankton grazing effects in microcosms, which will be
619 discussed in section 4. 23.2.

620

621 The measurement of photophysiological parameters revealed that the phytoplankton had generally better photosynthetic
622 performance in the slag and olivine treatments than in the control, especially after the phytoplankton bloom. During the
623 first 5 days, the changes in phytoplankton photosynthetic performance were indistinguishable amongst treatments between
624 the control and the slag treatment, while the values of α , ETR_{max} and F_v/F_m were lower in olivine treatment. At this time
625 aAll microcosms had similar health because of the relatively high NO_x^- concentrations and Fe supply (around 5 ± 00 nmol
626 L^{-1}), but the suspended particles in the olivine treatment may have led to artifacts in the measuring of photophysiology by
627 FRRf. Scattering and/or absorption of light by suspended olivine particles is the most parsimonious explanation for the
628 simultaneous depression in α , ETR_{max} and F_v/F_m . After day 5, the F_v/F_m , α and ETR_{max} values decreased significantly faster
629 in the control than in the treatments, and to values lower than the initial condition. A decrease of F_v/F_m is commonly
630 associated with physiological stress, such as nutrient limitation, and high light stress (Bhagooli, et al., 2021), with Fe
631 limitation causing a more pronounced decline in F_v/F_m than nitrogen limitation (Gorbunov, et al., 2021). The ETR_{max} , which
632 represents the maximum electron transport rate, has also been shown to be negatively affected when phytoplankton
633 experience nitrogen or Fe limitation (Kolber et al., 1994; Gorbunov & Falkowski 2021). Furthermore, the change in
634 photosynthesis performance after day 10 was suspected to be driven by the microphytoplankton because the decrease of
635 F_v/F_m , α , and ETR_{max} in the control was coupled with the decrease in microphytoplankton abundance while the other
636 phytoplankton groups were in low abundance as in the mineral addition treatments, and the microphytoplankton contributed
637 significantly (75 %) to community biovolume. All microcosms were similarly NO_x^- limited from day 5 onward (Fig. 3) so
638 that N-limitation is unlikely to explain different trends in photophysiological parameters between the control and OAE
639 treatments. Trace metals, especially Fe, released through slag and olivine additions could potentially explain these
640 differences.

641
642 Several of the trace metals released from slag and olivine are required for photosynthesis. For example, Fe is required for
643 many proteins functioning in photosynthesis, such as cytochromes, ferredoxin, and superoxide dismutase (SOD) (Twining
644 and Baines, 2013), and the addition of Fe can stimulate the growth of phytoplankton (Sunda and Huntsman, 1997) and
645 increase F_v/F_m (Behrenfeld et al., 2006). The dissolved and particulate Fe concentrations were higher in mineral addition
646 treatments than in the control indicating potentially more Fe available to sustain phytoplankton photosynthesis. While this
647 explanation is intriguing for the observed trends in photophysiology, it remains unclear why such strong differences
648 occurred between mineral addition and control treatments despite dissolved Fe concentrations of $\sim 5 \pm 00$ nmol L^{-1} at the end
649 of the experiment in the control. In Fe-limited ocean regions, dissolved Fe is at least two orders of magnitude lower, and
650 the enhancement of Fe to ~ 1.5 nmol L^{-1} can induce major phytoplankton blooms and relieve photophysiological stress (De
651 Baar et al., 2005). It is possible that these coastal phytoplankton species have higher Fe requirements than those from the
652 open ocean where Fe is limiting (Strzepek and Harrison, 2004). We speculate that when Fe was consumed during the
653 phytoplankton bloom, bioavailable Fe was much lower in the control, and may have been insufficient to meet the cellular
654 requirements of coastal phytoplankton. Our findings therefore suggest that Fe perturbations is not only relevant for lower
655 Fe open ocean regions but could also be relevant for coastal ocean locations.

656
657 Alternatively, the addition of Mn, Ni and other trace metals from mineral addition may have benefited photosynthesis.
658 Manganese is required for the water-splitting reaction of photosystem II (Armstrong, 2008), and both Mn and Ni are
659 common bioactive trace metals for SODs in marine phytoplankton. The noxious superoxide anion radical (O_2^-) generated
660 from aerobic respiration and oxygenic photosynthesis could be harmful to phytoplankton physiology, and SOD removes

661 O₂, thus improving photosynthesis (Wafar et al., 1995; Wolfe-Simon et al., 2005). This is consistent with our
662 photosynthetic measurements. Interestingly, although the amounts and types of trace metals released from the slag and
663 olivine powders were different, they led to relatively similar F_v/F_m values with only slightly higher F_v/F_m in the olivine
664 than the slag treatment from days 10-21. Over this time, these trace metal additions could have fertilized different
665 phytoplankton species ([Pausch et al., 2019](#); [Balaguer et al., 2022](#); [Guo et al., 2022](#)) possibly because different
666 phytoplankton could have different trace metal requirements, such as for SOD. For example, cyanobacteria have NiSOD,
667 diatoms have MnSOD, dinoflagellates have both FeSOD and MnSOD (Wolfe-Simon et al., 2005). Another explanation is
668 that phytoplankton in the control were limited by bicarbonate while the treatments had sufficient bicarbonate from added
669 minerals. However, we were unable to determine the species-level changes in the phytoplankton community, and hence
670 whether these trace metals, individually or combined, could account for the observed phytoplankton community
671 photosynthetic performance.

672

673 **4.34.2.2. OAE impacts on the zooplankton community**

674 Slag-based OAE did not significantly influence the zooplankton community composition while olivine-based OAE induced
675 some statistically significant effects, including a lower Shannon diversity. The increase in *N. scintillans* abundance and the
676 decrease in *Penilia* sp. and *Oikopleura* sp. in the olivine treatment indicate that the zooplankton response to OAE can vary
677 among different zooplankton types.

678

679 The observed lower abundance of *Oikopleura* sp. on day 13 in the olivine treatment may indicate a temporary suppression
680 or a slower growth rate of this zooplankton species in response to the olivine addition. This could be attributed to the
681 potential effects of olivine on the availability of essential nutrients or changes in the physicochemical environment of the
682 water. However, the subsequent increase in *Oikopleura* sp. abundance by day 22 suggests that the growth of this species
683 may have recovered or accelerated in the olivine treatment, leading to a higher abundance compared to the slag treatment
684 and the control on day 22. As discussed in section 4.2.1, reduced *Oikopleura* sp. abundance was unlikely due to reduced
685 food availability since phytoplankton within the preferred edible size spectrum, such as cyanobacteria and nanoeukaryotes,
686 were even more abundant in the olivine treatment. Instead, we hypothesize it to be an effect of the suspended olivine
687 particles that occurred for approximately the first 5 days of the study that were so plentiful that they turned the enclosed
688 seawater milky and may have clogged the mucous feeding mesh of *Oikopleura* sp. (Lombard et al., 2011).

689

690 The abundance of *Penilia* sp. and *Oikopleura* sp. was lower in the olivine treatment than the other two groups throughout
691 the experiment while the abundance of *N. scintillans* was consistently higher. The section second bloom of cyanobacteria
692 in olivine is likely to be the results of decreased predators, like *Penilia* sp. and *Oikopleura* sp., although the changes in
693 their abundance were not statistically significant between treatments and the control. We cannot provide a particularly
694 convincing hypothesis about what specifically drove these differences though it is tempting to speculate that suspended
695 particles present at the beginning may have played a role also for those organisms since this was the only apparent
696 systematic difference to the control and slag treatment. The proliferation of *N. scintillans* can be problematic since
697 heterotrophic dinoflagellate blooms can regulate phytoplankton communities, cause toxicity to aquatic fish, and create an
698 hypoxic sub-surface zone (Baliarsingh et al., 2016; Zhang et al., 2020; Al-Azri et al., 2007), although a bloom of *N.*
699 *scintillans* in southeast Australia only induced ichthyotoxicity when the cell concentration reached 2,000,000 cells L⁻¹

700 (Hallegraeff et al., 2019). For comparison, we observed a maximum of 32 cells L⁻¹ in one microcosm replicate of the olivine
701 treatment.

702

703 In comparison to olivine, steel slag seemed to have less potential to affect zooplankton community composition. The
704 abundance of all groups of phytoplankton, apart from microphytoplankton after day 10, was similar in the slag treatment
705 and the control through the experiment. This is probably because the amount of slag powder added in the treatment was
706 much less than the olivine powder resulting in fewer physical particle perturbations to zooplankton. In addition, the
707 chemistry perturbations such as enhanced alkalinity concentration and various dissolved trace metals, especially Mn, from
708 the slag powder did not seem to have a notable direct influence on zooplankton abundance over the three-week period.
709 Even though we did not observe drastic ~~zooplankton abundance~~ changes in zooplankton abundance during the experiment,
710 considering there was higher microphytoplankton abundance in the slag treatment after day 10, slag powder may benefit
711 some zooplankton especially those who feed on large phytoplankton on a longer time scale.

712

713 4.4.4.2.3. Dissolved trace metal accumulation in seawater and its environmental implications

714 The addition of olivine and slag as OAE source minerals released trace metals into the seawater, predominantly Al, Fe, Ni,
715 and Cu (olivine) as well as Al, Fe, and Mn (slag). The maximum measured concentrations for dissolved Al, Fe, Ni, Cu, and
716 Mn were 1093, 253, 77, 27, and 810 ~~1190, 500, 80, 30, and 820~~ nmol L⁻¹, respectively. The threshold values for drinking
717 water with health or aesthetic considerations by the Australian Drinking Water Guidelines for Al, Fe, Ni, Cu, and Mn are
718 7400, 5360, 340, 15600, and 1800 nmol L⁻¹, respectively (NRMMC~~mmme~~, 2022). All dissolved trace metal concentrations
719 measured herein are well below these health and aesthetic threshold values. In natural freshwater sources, the
720 concentrations of Al, Fe, Ni, Cu and Mn are generally less than 44000, 71400, 510, 156, and 25400 nmol L⁻¹
721 (NRMMC~~mmme~~, 2022). Although these natural water data were primarily derived from rivers and streams, they serve as
722 valuable references for evaluating trace metal release in our experiment. Thus, mineral additions to the microcosms as
723 simulated here did not increase thresholds for any of the measured trace metals beyond those that are considered safe for
724 drinking water quality, and they were within the trace metal concentration range in natural water. However, while these
725 guidelines on drinking water provide a good starting point on how to quantify ~~qualify~~ what OAE perturbation could be
726 considered “safe” and “unsafe” with regards to trace metals, it must be recognized that seawater is not drinking water and
727 that critical thresholds may be different in the latter.

728

729 The release of trace metals from OAE materials is considered to have relatively strong effects on biology, particularly in
730 the open ocean where trace metals usually occur in lower concentrations. For example, ~~the~~ oceanic Al, Fe, Ni, and Mn
731 concentrations are about 2, 0.5, 8, and 0.3 nmol L⁻¹ (Bruland and Lohan, 2003; Sohrin and Bruland, 2011). Previous
732 research on OAE-associated trace metal impacts on individual phytoplankton species grown in laboratory environments
733 has shown that concentration thresholds beyond which trace metal induces negative effects on fitness likely differ between
734 species (Guo et al., 2022; Hutchins et al., 2023; Xin et al., 2023). Indeed, our experiment with plankton communities
735 provides further support that several components of the planktonic food web are affected by OAE. However, our experiment
736 does not allow determining whether observed effects were primarily invoked by carbonate chemistry, macronutrient (P and
737 Si), or trace metal perturbations. Thus, dedicated experiments isolating the impact of these factors on plankton will be
738 required in the future.

739 4.5.4.2.4. Particulate trace metal accumulation in seawater and its environmental implications

740 The Derwent ~~estuary~~ Estuary (where we collected our plankton communities) was highly metal polluted due to industrial
741 practice (Macleod and Coughanowr, 2019). Both our dissolved and particulate trace metal data indicated high background
742 metal concentrations, especially for Fe and Zn. Furthermore, the metal:POC ratios found here (~~Fig. S5~~) are higher than
743 reported for open ocean studies or lab cultures. For example, the Fe:POC can vary from 2-136 $\mu\text{mol mol}^{-1}$ depending on
744 the cultured phytoplankton species and the environmental dissolved Fe concentration (Kulkarni et al., 2006; Sunda and
745 Huntsman, 1995; King et al., 2012; Boyd et al., 2015). In our results the Fe:POC values ranged from 1200 to 39 000 μmol
746 mol^{-1} , which may be due to the particulate trace metal richness of the Derwent Estuary (control) and/or the addition of
747 lithogenic particles (slag and olivine treatment). The presence of abiotic particulate metal sources creates challenges to
748 quantify metal quotas and then to evaluate metal accumulation effects on biological organisms.

749
750 Our study reveals that the added minerals enriched the particulate trace metal pools to various degrees. Consistent with the
751 dissolved trace metal data, the slag treatment was enriched with particulate Fe and Mn while the olivine treatment was
752 enriched with particulate Fe and Ni. The enhanced particulate Ni and Mn concentrations were higher than before mineral
753 additions and the control levels. This is in line with previous research which indicates a positive correlation between
754 particulate and dissolved trace metal concentrations (Gaulier et al., 2019).

755
756 Based on the amounts released through OAE as simulated here ~~in~~ (Fig. 4), it appears that Ni and Mn have the highest
757 potential to cause toxicity in certain marine organisms (Jakimska et al., 2011). These trace metals have the potential to
758 accumulate in marine organisms over time (bioaccumulation effects), and their increased concentrations in the food chain
759 can lead to adverse effects on the health and well-being of organisms at higher trophic levels (biomagnification effects).
760 ~~Previous research has shown the bioaccumulation of Ni on zooplankton (Villagran et al., 2019; El Metwally et al., 2022),~~
761 ~~oyster (Chouvelon et al., 2022), molluscs (Andra Oros, 2010), and fish (Blewett and Wood, 2015); Mn in zooplankton (El~~
762 ~~Metwally et al., 2022), Antarctic bivalve (Husmann et al., 2012), clams (O'mara et al., 2019), and juvenile turbot (Van~~
763 ~~Bussel et al., 2014). However, other studies revealed no biomagnification of Ni or Mn in the marine food webs (Sun et al.,~~
764 ~~2020; Chouvelon et al., 2019; Campbell et al., 2005; Mathews and Fisher, 2008). Since it usually requires two connected~~
765 ~~trophic levels be examined simultaneously (Colaço et al., 2006; Wang, 2002), it is hard to know whether the OAE-related~~
766 ~~trace metal addition will be biomagnified. In addition, the bioaccumulation and biomagnification do not necessary result~~
767 ~~in toxicity. Therefore, the~~ One crucial next step ~~is~~ will be to investigate whether the enhanced dissolved/particulate trace
768 metal will affect higher trophic levels to estimate the environmental risks of OAE on other marine organisms.

770 5 Conclusions

771 Our study aimed to assess the environmental impacts of two ground OAE minerals, olivine and steel slag, on coastal
772 plankton communities. Both minerals released alkalinity, leading to an elevation in pH_T . However, the addition of steel
773 slag exhibited significantly higher efficiency in elevating alkalinity compared to olivine.

774
775 Approximately 1.9 g L⁻¹ of olivine powder were added in the olivine treatments, leading to a 29 $\mu\text{mol kg}^{-1}$ increase in

776 alkalinity and increased concentrations of Si(OH)₄ and trace metals (Fe and Ni). Compared to this relatively modest
777 increase of alkalinity and associated Overall, the application of olivine powder had a noticeable effect on the coastal
778 plankton community. When comparing this impact to the visible perturbation of the plankton community (the seawater
779 turned highly turbid for about 4 days), the impact appears to be modest. Under real world conditions, dilution through
780 physical mixing with unperturbed water would further mitigate the perturbation. However, when comparing the impact on
781 the plankton community to the limited alkalinity enhancement and CO₂ removal potential, the impacts on the plankton
782 community that was achieved by adding 1.9 g L⁻¹ of olivine powder, it appears to be relatively pronounced. Thus,
783 although While our experiment was ran for only 3 weeks, and olivine powder may slowly release more alkalinity, the short-
784 term response monitored here suggests that the immediate climatic benefit is relatively small compared to a relatively
785 pronounced environmental effect.

786
787 In general, the addition of steel slag powder had limited influence on both the phytoplankton and zooplankton community.
788 Only 0.038 g L⁻¹ of slag were added to the treatment but this led to an alkalinity enhancement of 361 μmol kg⁻¹ and the
789 increased concentrations of macronutrients (P and Si) and trace metals (Mn and Fe) additions as well as changes in
790 carbonate chemistry, and some of these perturbations occurred rapidly. Although limited environmental impacts were
791 observed from the slag treatment in our experiment, if slag powders were applied at large scale in the field, these
792 perturbations may circulate in the ocean and influence plankton community well beyond the experimental sites some aspects
793 require further study. For example, the pronounced release of P could cause eutrophication and the relatively rapid increase
794 in pH may be a detrimental aspect if organisms cannot acclimate fast enough. Furthermore, it is essential to consider that
795 the composition of steel slag can vary depending on the source factory (Wang et al., 2011; Proctor et al., 2000), which may
796 affect the efficiency of carbon removal and change the trace metal perturbation. Nevertheless, just based on our experiment,
797 the comparison between the immediate climatic benefit and environmental effect appears to be more favourable for slag
798 than olivine.

799
800 Based on our findings, it can be concluded that steel slag powder exhibited fewer environmental impacts on plankton
801 communities compared to olivine powder, considering relative to its capacity for alkalinity enhancement. The results
802 highlight the importance of carefully assessing the environmental consequences of using specific OAE minerals,
803 particularly when considering their potential effects on plankton communities.

804
805 **Data availability.** Data are available in the Institute for Marine and Antarctic Studies (IMAS) data catalogue, University
806 of Tasmania (UTAS) (<https://doi.org/10.25959/X6FH-9K15>, Guo, J., & Bach, L. (2023).).

807
808 **Author contributions.** LTB, RFS, KMS and JAG designed the experiments and JAG carried them out. LTB, RFS and
809 KMS supervised the study. ATT analysed the dissolved/particulate trace metal samples. JAG conducted statistical analyses.
810 JAG prepared the manuscript with contributions from all authors.

811
812 **Competing interests.** The contact author has declared that none of the authors has any competing interests.

813
814 **Disclaimer.** Publisher's note: Copernicus Publications remains neutral with regard to jurisdictional claims in published
815 maps and institutional affiliations.

816

817 **Acknowledgements.** We would like to thank Steve Van Orsouw from Moyne Shire Council, Victoria, Australia for
818 providing olivine rocks. We also thank Bradley Mansell who provided the Basic Oxygen Slag from Liberty Primary Steel
819 Whyalla Steelworks in Whyalla, South Australia, Australia.- We ~~appreciate~~ thank Sandrin Feig and Thomas Rodemann for
820 their support on scanning electron microscopy and particulate organic matter. We appreciate the assistance of Pam Quayle
821 and Axel Durand (IMAS) in the lab, particularly with particulate metal digestions.

822

823 **Financial support.** This research has been supported by the Australian Research Council through a Future Fellowship
824 ~~awarded to Lennart Thomas Bach~~ (project ~~(FT200100846 to LTB)~~, ~~the Carbon to Sea Initiative (LTB)~~, and by the Australian
825 Antarctic Program Partnership (ASCI000002 to RFS, KMS and JAG). Access to SF-ICP-MS instrumentation was
826 facilitated through ARC LIEF funding (LE0989539) awarded to ATT. ~~JAG was thanks~~ the Australian Research Training
827 Program (RTP) for her scholarship.

828 References

- 829 Ackerman, L., Jelínek, E., Medaris, G., Ježek, J., Siebel, W., and Strnad, L.: Geochemistry of Fe-rich peridotites and
830 associated pyroxenites from Horní Bory, Bohemian Massif: Insights into subduction-related melt–rock reactions,
831 Chem. Geol., 259, 152-167, <https://doi.org/10.1016/j.chemgeo.2008.10.042>, 2009.
- 832 Al-Azri, A., Al-Hashmi, K., Goes, J., Gomes, H., Rushdi, A. I., Al-Habsi, H., Al-Khusaibi, S., Al-Kindi, R., and Al-Azri, N.:
833 Seasonality of the bloom-forming heterotrophic dinoflagellate *Noctiluca scintillans* in the Gulf of Oman in relation
834 to environmental conditions, Int. J. Oceans Oceanogr., 2, 51-60, 2007.
- 835 ~~Andra Oros, M. T. G.: Comparative data in the accumulation of five heavy metals (cadmium, chromium, copper, nickel,~~
836 ~~lead) in some marine species (mollusks, fish) from the Romanian Sector of the Black Sea, Recherches Marines, 39,~~
837 ~~89-108, 2010.~~
- 838 Armstrong, F. A.: Why did nature choose manganese to make oxygen?, Philos Trans R Soc Lond B Biol Sci, 363, 1263-1270,
839 <https://doi.org/10.1098/rstb.2007.2223>, 2008.
- 840 Bach, L. T., Gill, S. J., Rickaby, R. E. M., Gore, S., and Renforth, P.: CO2 removal with enhanced weathering and ocean
841 alkalinity enhancement: potential risks and co-benefits for marine pelagic ecosystems, Front Clim, 1, 1-21,
842 <http://doi.org/10.3389/fclim.2019.00007>, 2019.
- 843 Balaguer, J., Koch, F., Hassler, C. et al.: Iron and manganese co-limit the growth of two phytoplankton groups dominant at
844 two locations of the Drake Passage. Commun Biol 5, 207, <https://doi.org/10.1038/s42003-022-03148-8>, 2022.
- 845 Baliarsingh, S. K., Lotliker, A. A., Trainer, V. L., Wells, M. L., Parida, C., Sahu, B. K., Srichandan, S., Sahoo, S., Sahu, K. C., and
846 Kumar, T. S.: Environmental dynamics of red *Noctiluca scintillans* bloom in tropical coastal waters, Mar. Pollut. Bull.,
847 111, 277-286, <https://doi.org/10.1016/j.marpolbul.2016.06.103>, 2016.
- 848 Basu, S. and Mackey, K. R. M.: Phytoplankton as key mediators of the biological carbon pump: their responses to a
849 changing climate, Sustainability, 10, 869, <https://doi.org/10.3390/su10030869>, 2018.
- 850 Behrenfeld, M. J., Worthington, K., Sherrell, R. M., Chavez, F. P., Strutton, P., McPhaden, M., and Shea, D. M.: Controls on
851 tropical Pacific Ocean productivity revealed through nutrient stress diagnostics, Nature, 442, 1025-1028,
852 <https://doi.org/10.1038/nature05083>, 2006.
- 853 ~~Blewett, T. A. and Wood, C. M.: Salinity dependent nickel accumulation and oxidative stress responses in the euryhaline~~
854 ~~killifish (*Fundulus heteroclitus*), Arch Environ Contam Toxicol, 68, 382-394, [http://doi.org/10.1007/s00244-014-](http://doi.org/10.1007/s00244-014-0115-6)~~
855 ~~0115-6, 2015.~~
- 856 Bowie, A. R., Townsend, A. T., Lannuzel, D., Remenyi, T. A., and van der Merwe, P.: Modern sampling and analytical
857 methods for the determination of trace elements in marine particulate material using magnetic sector inductively
858 coupled plasma-mass spectrometry, Anal Chim Acta, 676, 15-27, <https://doi.org/10.1016/j.aca.2010.07.037>, 2010.
- 859 Boyd, P. W., Strzepek, R. F., Ellwood, M. J., Hutchins, D. A., Nodder, S. D., Twining, B. S., and Wilhelm, S. W.: Why are biotic
860 iron pools uniform across high- and low-iron pelagic ecosystems?, Global Biogeochem. Cycles, 29, 1028-1043,
861 <http://doi.org/10.1002/2014gb005014>, 2015.
- 862 Boyd, P. W., Jickells, T., Law, C., Blain, S., Boyle, E., Buesseler, K., Coale, K., Cullen, J., De Baar, H. J., and Follows, M.:
863 Mesoscale iron enrichment experiments 1993-2005: synthesis and future directions, Science, 315, 612-617,
864 <http://doi.org/10.1126/science.1131669>, 2007.

865 Bruland, K. W. and Lohan, M. C.: 6.02 Controls of Trace Metals in Seawater, in: Treatise on Geochemistry, edited by:
866 Elderfield, H., Holland, H. D., and Turekian, K. K., Elsevier Pergamon, 23-47, [http://doi.org/10.1016/b0-08-043751-](http://doi.org/10.1016/b0-08-043751-6/06105-3)
867 [6/06105-3](http://doi.org/10.1016/b0-08-043751-6/06105-3), 2003.

868 Burt, D. J., Fröb, F., and Ilyina, T.: The sensitivity of the marine carbonate system to regional ocean alkalinity enhancement,
869 *Front Clim*, 3, <http://doi.org/10.3389/fclim.2021.624075>, 2021.

870 ~~Campbell, L. M., Norstrom, R. J., Hobson, K. A., Muir, D. C., Backus, S., and Fisk, A. T.: Mercury and other trace elements
871 in a pelagic Arctic marine food web (Northwater Polynya, Baffin Bay), *Sci Total Environ*, 351-352, 247-263,
872 <http://doi.org/10.1016/j.scitotenv.2005.02.043>, 2005.~~

873 Caserini, S., Storni, N., and Grosso, M.: The availability of limestone and other raw materials for ocean alkalinity
874 enhancement, *Global Biogeochem. Cycles*, 36, <http://doi.org/10.1029/2021gb007246>, 2022.

875 ~~Chouvelon, T., Strady, E., Harmelin-Vivien, M., Radakovitch, O., Brach-Papa, C., Crochet, S., Knoery, J., Rozuel, E., Thomas,
876 B., Tronczynski, J., and Chiffolleau, J. F.: Patterns of trace metal bioaccumulation and trophic transfer in a
877 phytoplankton-zooplankton-small pelagic fish marine food web, *Mar. Pollut. Bull.*, 146, 1013-1030,
878 <http://doi.org/10.1016/j.marpolbul.2019.07.047>, 2019.~~

879 ~~Chouvelon, T., Aubry, I., Mornet, L., Bruzac, S., Charlier, K., Araújo, D. F., Gonzalez, J. L., Gonzalez, P., Gourves, P.-Y.,
880 Méteignier, C., Perrière-Rumèbe, M., Rigouin, L., Rozuel, E., Savoye, N., Sireau, T., and Akcha, F.: Role of suspended
881 particulate material on growth and metal bioaccumulation in oysters (*Crassostrea gigas*) from a French coastal
882 semi-enclosed production area, Arcachon Bay, *J. Mar. Syst.*, 234, 103778,
883 <https://doi.org/10.1016/j.jmarsys.2022.103778>, 2022.~~

884 ~~Colaço, A., Bustamante, P., Fouquet, Y., Sarradin, P. M., and Serrão-Santos, R.: Bioaccumulation of Hg, Cu, and Zn in the
885 Azores triple junction hydrothermal vent fields food web, *Chemosphere*, 65, 2260-2267,
886 <http://doi.org/10.1016/j.chemosphere.2006.05.034>, 2006.~~

887 De Baar, H. J., Boyd, P. W., Coale, K. H., Landry, M. R., Tsuda, A., Assmy, P., Bakker, D. C., Bozec, Y., Barber, R. T., and Brzezinski,
888 M. A.: Synthesis of iron fertilization experiments: from the iron age in the age of enlightenment, *J Geophys Res*
889 *Oceans*, 110, <https://doi.org/10.1029/2004JC002601>, 2005.

890 Dickson, A. G., Sabine, C. L., and Christian, J. R.: Guide to best practices for ocean CO₂ measurements, North Pacific Marine
891 Science Organization, Canada2007.

892 Egge, J. and Jacobsen, A.: Influence of silicate on particulate carbon production in phytoplankton, *Mar. Ecol. Prog. Ser.*,
893 147, 219-230, <http://doi.org/10.3354/meps147219>, 1997.

894 ~~El-Metwally, M. E., Abu-El-Regal, M. A., Abdelkader, A. I., and Sanad, E. F.: Heavy metal accumulation in zooplankton and
895 impact of water quality on its community structure, *Arab. J. Geosci.*, 15, 1-14, [https://doi.org/10.1007/s12517-021-](https://doi.org/10.1007/s12517-021-09424-x)
896 [09424-x](https://doi.org/10.1007/s12517-021-09424-x), 2022.~~

897 Evans, C., O'Reilly, J. E., and Thomas, J.: A handbook for the measurement of chlorophyll and primary production, 1987.

898 Falkowski, P. G.: The role of phytoplankton photosynthesis in global biogeochemical cycles, *Photosynthesis Research*, 39,
899 235-258, <https://doi.org/10.1007/BF00014586>, 1994.

900 Feng, E. Y., Koeve, W., Keller, D. P., and Oschlies, A.: Model-based assessment of the CO₂ sequestration potential of coastal
901 ocean alkalization, *Earth's Future*, 5, 1252-1266, <http://doi.org/10.1002/2017ef000659>, 2017.

902 Ferderer, A., Chase, Z., Kennedy, F., Schulz, K. G., and Bach, L. T.: Assessing the influence of ocean alkalinity enhancement
903 on a coastal phytoplankton community, *Biogeosciences*, 19, 5375-5399, <http://doi.org/10.5194/bg-19-5375-2022>,
904 2022.

905 Ferderer, A., Schulz, K. G., Riebesell, U., Baker, K. G., Chase, Z., and Bach, L. T.: Investigating the effect of silicate and calcium
906 based ocean alkalinity enhancement on diatom silicification, *Biogeosciences Discuss.* [preprint],
907 <https://doi.org/10.5194/bg-2023-144>, in review, 2023.

908 Package 'seacarb'-Seawater Carbonate Chemistry: <https://cran.r-project.org/web/packages/seacarb/index.html>, last
909 access: 2023/6/1.

910 Gaulier, C., Zhou, C., Guo, W., Bratkic, A., Superville, P. J., Billon, G., Baeyens, W., and Gao, Y.: Trace metal speciation in
911 North Sea coastal waters, *Sci. Total Environ.*, 692, 701-712, <http://doi.org/10.1016/j.scitotenv.2019.07.314>, 2019.

912 Guo, J., Bao, Y., and Wang, M.: Steel slag in China: Treatment, recycling, and management, *Waste Management*, 78, 318-
913 330, <https://doi.org/10.1016/j.wasman.2018.04.045>, 2018.

914 Guo, J. A., Strzepak, R., Willis, A., Ferderer, A., and Bach, L. T.: Investigating the effect of nickel concentration on
915 phytoplankton growth to assess potential side-effects of ocean alkalinity enhancement, *Biogeosciences*, 19, 3683-
916 3697, <https://doi.org/10.5194/bg-19-3683-2022>, 2022.

917 Hallegraeff, G. M., Albinsson, M. E., Dowdney, J., Holmes, A. K., Mansour, M. P., and Seger, A.: Prey preference,
918 environmental tolerances and ichthyotoxicity by the red-tide dinoflagellate *Noctiluca scintillans* cultured from
919 Tasmanian waters, *J. Plankton Res.*, 41, 407-418, <https://doi.org/10.1093/plankt/fbz037>, 2019.

920 Hansen, H. P. and Koroleff, F.: Determination of nutrients, in: *Methods of seawater analysis*, edited by: Grasshoff, K.,
921 Kremling, K., and Ehrhardt, M., 159-228, <https://doi.org/10.1002/9783527613984.ch10>, 1999.

922 Hartmann, J., West, A. J., Renforth, P., Köhler, P., De La Rocha, C. L., Wolf-Gladrow, D. A., Dürr, H. H., and Scheffran, J.:
923 Enhanced chemical weathering as a geoengineering strategy to reduce atmospheric carbon dioxide, supply
924 nutrients, and mitigate ocean acidification, *Rev. Geophys.*, 51, 113-149, <http://doi.org/10.1002/rog.20004>, 2013.

925 Humphreys, M. P., Lewis, E. R., Sharp, J. D., and Pierrot, D.: PyCO2SYS v1. 8: marine carbonate system calculations in
926 Python, *Geosci Model Dev*, 15, 15-43, <https://doi.org/10.5194/gmd-15-15-2022>, 2022.

927 ~~Husmann, G., Abele, D., Monien, D., Monien, P., Kriews, M., and Philipp, E. E. R.: The influence of sedimentation on metal
928 accumulation and cellular oxidative stress markers in the Antarctic bivalve *Laternula elliptica*, *Estuar Coast Shelf
929 Sci*, 111, 48-59, <http://doi.org/10.1016/j.ecss.2012.06.003>, 2012.~~

930 Hutchins, D. A., Fu, F.-X., Yang, S.-C., John, S. G., Romaniello, S. J., Andrews, M. G., and Walworth, N. G.: [Responses of](#)
931 [globally important phytoplankton species to olivine dissolution products and implications for carbon dioxide](#)
932 [removal via ocean alkalinity enhancement](#), *Biogeosciences*, 20, 4669-4682, [https://doi.org/10.5194/bg-20-4669-](https://doi.org/10.5194/bg-20-4669-2023)
933 ~~2023.~~ [Responses of globally important phytoplankton groups to olivine dissolution products and implications](#)
934 [for carbon dioxide removal via ocean alkalinity enhancement](#), *bioRxiv* [preprint],
935 <https://doi.org/10.1101/2023.04.08.536121>, 2023.

936 Ilyina, T., Wolf-Gladrow, D., Munhoven, G., and Heinze, C.: Assessing the potential of calcium-based artificial ocean
937 alkalinization to mitigate rising atmospheric CO₂ and ocean acidification, *Geophys. Res. Lett.*, 40, 5909-5914,
938 <https://doi.org/10.1002/2013GL057981>, 2013.

939 Jakimska, A., Konieczka, P., Skóra, K., and Namieśnik, J.: Bioaccumulation of metals in tissues of marine animals, Part II:
940 metal concentrations in animal tissues, *Pol J Environ Stud*, 20, 2011.

941 Keller, D. P., Feng, E. Y., and Oschlies, A.: Potential climate engineering effectiveness and side effects during a high carbon
942 dioxide-emission scenario, *Nat. Commun.*, 5, 3304, <https://doi.org/10.1038/ncomms4304>, 2014.

943 King, A. L., Sañudo-Wilhelmy, S. A., Boyd, P. W., Twining, B. S., Wilhelm, S. W., Breene, C., Ellwood, M. J., and Hutchins, D.
944 A.: A comparison of biogenic iron quotas during a diatom spring bloom using multiple approaches, *Biogeosciences*,
945 9, 667-687, <http://doi.org/10.5194/bg-9-667-2012>, 2012.

946 Kohler, P., Hartmann, J., and Wolf-Gladrow, D. A.: Geoengineering potential of artificially enhanced silicate weathering of
947 olivine, *Proc. Natl. Acad. Sci. USA*, 107, 20228-20233, <https://doi.org/10.1073/pnas.1000545107>, 2010.

948 Kourounis, S., Tsvivilis, S., Tsakiridis, P. E., Papadimitriou, G. D., and Tsi bouki, Z.: Properties and hydration of blended
949 cements with steelmaking slag, *Cem. Concr. Res.*, 37, 815-822, <https://doi.org/10.1016/j.cemconres.2007.03.008>,
950 2007.

951 Kulkarni, P. P., She, Y. M., Smith, S. D., Roberts, E. A., and Sarkar, B.: Proteomics of metal transport and metal-associated
952 diseases, *Chemistry*, 12, 2410-2422, <http://doi.org/10.1002/chem.200500664>, 2006.

953 Lenton, A., Matear, R. J., Keller, D. P., Scott, V., and Vaughan, N. E.: Assessing carbon dioxide removal through global and
954 regional ocean alkalinization under high and low emission pathways, *Earth. Syst. Dyn.*, 9, 339-357,
955 <https://doi.org/10.5194/esd-9-339-2018>, 2018.

956 Lombard, F., Selander, E., and Kjørboe, T.: Active prey rejection in the filter-feeding appendicularian *Oikopleura dioica*,
957 *Limnol. Oceanogr.*, 56, 1504-1512, <http://doi.org/10.4319/lo.2011.56.4.1504>, 2011.

958 Lueker, T. J., Dickson, A. G., and Keeling, C. D.: Ocean pCO₂ calculated from dissolved inorganic carbon, alkalinity, and
959 equations for K₁ and K₂: validation based on laboratory measurements of CO₂ in gas and seawater at equilibrium,
960 *Mar. Chem.*, 70, 105-119, [https://doi.org/10.1016/S0304-4203\(00\)00022-0](https://doi.org/10.1016/S0304-4203(00)00022-0), 2000.

961 Macleod, C. and Coughanowr, C.: Heavy metal pollution in the Derwent estuary: History, science and management, *Reg.*
962 *Stud. Mar. Sci.*, 32, <http://doi.org/10.1016/j.risma.2019.100866>, 2019.

963 ~~Mathews, T. and Fisher, N. S.: Trophic transfer of seven trace metals in a four-step marine food chain, *Mar. Ecol. Prog. Ser.*,
964 367, 23-33, <http://doi.org/10.3354/meps07536>, 2008.~~

965 Moore, C. M., Mills, M. M., Arrigo, K. R., Berman-Frank, I., Bopp, L., Boyd, P. W., Galbraith, E. D., Geider, R. J., Guieu, C.,
966 Jaccard, S. L., Jickells, T. D., La Roche, J., Lenton, T. M., Mahowald, N. M., Marañón, E., Marinov, I., Moore, J. K.,
967 Nakatsuka, T., Oschlies, A., Saito, M. A., Thingstad, T. F., Tsuda, A., and Ulloa, O.: Processes and patterns of oceanic
968 nutrient limitation, *Nat. Geosci.*, 6, 701-710, <http://doi.org/10.1038/ngeo1765>, 2013.

969 Nelson, D. M., Smith Jr, W. O., Muench, R. D., Gordon, L. I., Sullivan, C. W., and Husby, D. M.: Particulate matter and nutrient
970 distributions in the ice-edge zone of the Weddell Sea: relationship to hydrography during late summer, *Deep. Sea.*
971 *Res. A*, 36, 191-209, [https://doi.org/10.1016/0198-0149\(89\)90133-7](https://doi.org/10.1016/0198-0149(89)90133-7), 1989.

972 NRMCM, N. a.: The Australian Drinking Water Guidelines (2011) - Version 3.8 Updated 2022, 2022.

973 ~~Ó'Mara, K., Adams, M., Burford, M. A., Fry, B., and Cresswell, T.: Uptake and accumulation of cadmium, manganese and
974 zinc by fisheries species: Trophic differences in sensitivity to environmental metal accumulation, *Sci. Total Environ.*,
975 690, 867-877, <http://doi.org/10.1016/j.scitotenv.2019.07.016>, 2019.~~

976 [Pausch, F., Bischof, K., Trimborn, S.: Iron and manganese co-limit growth of the Southern Ocean diatom *Chaetoceros debilis*.](#)
977 [PLOS ONE 14, e0221959. <https://doi.org/10.1371/journal.pone.0221959>, 2019.](#)

978 Paquay, F. S. and Zeebe, R. E.: Assessing possible consequences of ocean liming on ocean pH, atmospheric CO₂

979 concentration and associated costs, *Int. J. Greenh. Gas Control.*, 17, 183-188,
980 <https://doi.org/10.1016/j.ijggc.2013.05.005>, 2013.

981 Platt, T., Gallegos, C. L., and Harrison, W. G.: Photoinhibition of photosynthesis in natural assemblages of marine
982 phytoplankton, *J. Mar. Res.*, 38, 687-701, 1980.

983 Proctor, D. M., Fehling, K. A., Shay, E. C., Wittenborn, J. L., Green, J. J., Avent, C., Bigham, R. D., Connolly, M., Lee, B.,
984 Shepker, T. O., and Zak, M. A.: Physical and chemical characteristics of blast furnace, basic oxygen furnace, and
985 electric arc furnace steel industry slags, *Environ. Sci. Technol.*, 34, 1576-1582, <http://doi.org/10.1021/es9906002>,
986 2000.

987 Reichl, C., Schatz, M., and Zsak, G.: World mining data, 1-261, 2018.

988 Renforth, P.: The negative emission potential of alkaline materials, *Nat. Commun.*, 10, <http://doi.org/10.1038/s41467-019-09475-5>, 2019.

989 Renforth, P. and Henderson, G.: Assessing ocean alkalinity for carbon sequestration, *Rev. Geophys.*, 55, 636-674,
990 <http://doi.org/10.1002/2016rg000533>, 2017.

991 Schallenberg, C., Strzepek, R. F., Schuback, N., Clementson, L. A., Boyd, P. W., and Trull, T. W.: Diel quenching of Southern
992 Ocean phytoplankton fluorescence is related to iron limitation, *Biogeosciences*, 17, 793-812,
993 <https://doi.org/10.5194/bg-17-793-2020>, 2020.

994 Schuiling, R. D. and Krijgsman, P.: Enhanced weathering: an effective and cheap tool to sequester CO₂, *Clim. Change*, 74,
995 349-354, <https://doi.org/10.1007/s10584-005-3485-y>, 2006.

996 Selfe, C.: Developing Transfer Function to Measuring Phytoplankton Cellular Properties with Flow Cytometry, Master's
997 thesis, Institute of Marine and Antarctic Studies, University of Tasmania, Australia, 2022.

998 Comparing smooths in factor-smooth interactions II ordered factors:
999 <https://fromthebottomoftheheap.net/2017/12/14/difference-splines-ii/>, last access: March 2023.

1000 Smith, S. M., Geden, O., Nemet, G. F., Gidden, M. J., Lamb, W. F., Powis, C., Bellamy, R., Callaghan, M. W., Cowie, A., Cox,
1001 E., Fuss, S., Gasser, T., Grassi, G., Greene, J., Lück, S., Mohan, A., Müller-Hansen, F., Peters, G. P., Pratama, Y., Repke,
1002 T., Riahi, K., Schenuit, F., Steinhäuser, J., Strefler, J., Valenzuela, J. M., and Minx, J. C.: The State of Carbon Dioxide
1003 Removal - 1st Edition, <http://doi.org/10.17605/OSF.IO/W3B4Z>, 2023.

1004 Sohrin, Y. and Bruland, K. W.: Global status of trace elements in the ocean, *TrAC, Trends Anal. Chem.*, 30, 1291-1307,
1005 <https://doi.org/10.1016/j.trac.2011.03.006>, 2011.

1006 Strzepek, R. F. and Harrison, P. J.: Photosynthetic architecture differs in coastal and oceanic diatoms, *Nature*, 431, 689-
1007 692, <http://doi.org/10.1038/nature02954>, 2004.

1008 Su, B., Chen, Y., Guo, S., and Liu, J.: Origins of orogenic dunites: petrology, geochemistry, and implications, *Gondwana Res.*,
1009 29, 41-59, <https://doi.org/10.1016/j.gr.2015.08.001>, 2016.

1010 Subhas, A. V., Marx, L., Reynolds, S., Flohr, A., Mawji, E. W., Brown, P. J., and Cael, B.: Microbial ecosystem responses to
1011 alkalinity enhancement in the North Atlantic Subtropical Gyre, *Front Clim*, 4,
1012 <https://doi.org/10.3389/fclim.2022.784997>, 2022.

1013 ~~Sun, T., Wu, H., Wang, X., Ji, C., Shan, X., and Li, F.: Evaluation on the biomagnification or biodilution of trace metals in
1014 global marine food webs by meta-analysis, *Environ. Pollut.*, 264, 113856,
1015 <http://doi.org/10.1016/j.envpol.2019.113856>, 2020.~~

1016 Sunda, W. G.: Trace metal-phytoplankton interactions in aquatic systems, in: *Environmental Microbe - Metal Interactions*,
1017 edited by: Lovley, D. R., 79-107, <https://doi.org/10.1128/9781555818098.ch4>, 2000.

1018 Sunda, W. G.: Feedback interactions between trace metal nutrients and phytoplankton in the ocean, *Frontiers in*
1019 *Microbiology*, 3, 1-22, <http://doi.org/10.3389/fmicb.2012.00204>, 2012.

1020 Sunda, W. G. and Huntsman, S. A.: Iron Uptake and Growth Limitation in Oceanic and Coastal Phytoplankton, *Marine*
1021 *Chemistry*, 50, 189-206, Doi 10.1016/0304-4203(95)00035-P, 1995.

1022 Sunda, W. G. and Huntsman, S. A.: Interrelated influence of iron, light and cell size on marine phytoplankton growth,
1023 *Nature*, 390, 389-392, <http://doi.org/10.1038/37093>, 1997.

1024 Tang, D. G. and Morel, F. M. M.: Distinguishing between cellular and Fe-oxide-associated trace elements in phytoplankton,
1025 *Mar. Chem.*, 98, 18-30, <http://doi.org/10.1016/j.marchem.2005.06.003>, 2006.

1026 ~~Tovar-Sanchez, A., Sanudo-Wilhelmy, S. A., Garcia-Vargas M., Weaver R. S., Popels L. C., and Hutchins D. A.: A trace metal
1027 clean reagent to remove surface-bound iron from marine phytoplankton. *Mar. Chem.*, 82, 1-2, 91-99,
1028 [https://doi.org/10.1016/S0304-4203\(03\)00054-9](https://doi.org/10.1016/S0304-4203(03)00054-9), 2003.~~

1029 Twining, B. S. and Baines, S. B.: The trace metal composition of marine phytoplankton, *Ann. Rev. Mar. Sci.*, 5, 191-215,
1030 <http://doi.org/10.1146/annurev-marine-121211-172322>, 2013.

1031 ~~van Bussel, C. G. J., Schroeder, J. P., Mahlmann, L., and Schulz, C.: Aquatic accumulation of dietary metals (Fe, Zn, Cu, Co,
1032 Mn) in recirculating aquaculture systems (RAS) changes body composition but not performance and health of
1033 juvenile turbot (*Psetta maxima*), *Aquacult. Eng.*, 61, 35-42, <https://doi.org/10.1016/j.aquaeng.2014.05.003>, 2014.~~

1034 ~~Villagran, D. M., Severini, M. D. F., Biancalana, F., Spetter, C. V., Fernandez, E. M., and Marcovecchio, J. E.: Bioaccumulation~~
1035

1036
1037
1038
1039
1040
1041
1042
1043
1044
1045
1046
1047
1048
1049
1050
1051
1052

~~of heavy metals in mesozooplankton from a human-impacted south western Atlantic estuary (Argentina), *J. Mar. Res.*, 77, 217-241, <http://doi.org/10.1357/002224019826887362>, 2019.~~

- Wafar, M., Le Corre, P., and L'Helguen, S.: f-Ratios calculated with and without urea uptake in nitrogen uptake by phytoplankton, *Deep Sea Res. I Oceanogr. Res. Pap.*, 42, 1669-1674, [https://doi.org/10.1016/0967-0637\(95\)00066-F](https://doi.org/10.1016/0967-0637(95)00066-F), 1995.
- Wang, Q., Yan, P., and Feng, J.: A discussion on improving hydration activity of steel slag by altering its mineral compositions, *J. Hazard. Mater.*, 186, 1070-1075, <https://doi.org/10.1016/j.jhazmat.2010.11.109>, 2011.
- Wang, W.: Interactions of trace metals and different marine food chains, *Mar. Ecol. Prog. Ser.*, 243, 295-309, <http://doi.org/10.3354/meps243295>, 2002.
- Wolfe-Simon, F., Grzebyk, D., Schofield, O., and Falkowski, P. G.: The role and evolution of superoxide dismutases in algae, *J. Phycol.*, 41, 453-465, <https://doi.org/10.1111/j.1529-8817.2005.00086.x>, 2005.
- Xin, X., Faucher, G., and Riebesell, U.: Phytoplankton response to Increased nickel in the context of ocean alkalinity enhancement, *Biogeosciences* [preprint], <https://doi.org/10.5194/bg-2023-130>, 2023.
- Zhang, W., Dong, Z., Zhang, C., Sun, X., Hou, C., Liu, Y., Wang, L., Ma, Y., and Zhao, J.: Effects of physical-biochemical coupling processes on the *Noctiluca scintillans* and *Mesodinium* red tides in October 2019 in the Yantai nearshore, China, *Mar. Pollut. Bull.*, 160, 111609, <https://doi.org/10.1016/j.marpolbul.2020.111609>, 2020.